Angewandte Chemie
Eine Zeitschrift der Gesellschaft Deutscher Chemiker

Supporting Information

Raman Microspectroscopic Evidence for the Metabolism of a Tyrosine Kinase Inhibitor, Neratinib, in Cancer Cells

Karim Aljakouch[+], Tatjana Lechtonen[+], Hesham K. Yosef[+], Mohamad K. Hammoud, Wissam Alsaidi, Carsten Kötting, Carolin Mügge, Robert Kourist, Samir F. El-Mashtoly, and Klaus Gerwert*

anie_201803394_sm_miscellaneous_information.pdf

EXPERIMENTAL SECTION

Cell Culture

Human HER2-positive breast adenocarcinoma cells, SK-BR-3 (HTB-30), and NSCLC cells NCI-H1975 (CRL-5908) and Calu-3 (HTB-55) cells were obtained from the American Type Culture Collection. Cells were cultured in Dulbecco's modified Eagle's medium (DMEM; Invitrogen, Carlsbad, USA) supplemented with 10% fetal bovine serum (FBS; Invitrogen, Carlsbad, USA), 2 mM L-glutamine, and 5% penicillin/streptomycin, and incubated at 37°C in 10% CO_2 atmosphere. Cells were seeded and grown on CaF_2 windows with grids (Korth Kristalle, Kiel, Germany) pretreated with 0.01% (w/v) poly-L-Lysine (Sigma-Aldrich GmbH, Munich, Germany). CaF_2 windows were used to avoid background signals from conventional glass slides. Cells were incubated with 10, 5, 1, and 0.5 µM of neratinib (HKI-272; Selleckchem, Munich, Germany) for 8 hours, which were directly followed by cell fixation using 3.5% paraformaldehyde (VWR International, Darmstadt, Germany). Finally, cells were submerged in phosphate-buffered saline (PBS; Invitrogen, Carlsbad, USA) and were stored at 4°C until used. The CaF_2 slides with grids allowed us to find the same cells at different microscopes.

Confocal Raman Microscopy

Raman micro-spectroscopic imaging was performed using a WITec alpha 300RA confocal Raman microscope (Ulm, Germany) as described previously.[1,2] A single-frequency diode laser of 785 nm (Toptica Photonics AG, Munich, Germany) was used as excitation source with an output power of approximately 300 mW. The laser radiation was coupled into a Zeiss microscope through a wavelength-specific single-mode optical fibre. The laser beam was collimated via an achromatic lens and passed through a holographic band-pass filter before being focused on the sample through a Nikon NIR APO (60×/1.00 NA) water-immersion objective. The laser excitation spot size is ~1 µm. The sample was located on a

piezoelectrically driven microscope scanning stage of an *x*,*y* resolution of ~3 ±5 nm and *z* resolution of ~0.3±2 nm. Raman back-scattered light was collected through a microscopic objective and passed through a holographic edge filter onto a multimode fibre (50 μm diameter) and into a 300 mm focal length monochromator, which incorporated a 600/mm grating blazed at 750 nm. Raman spectra were detected by a back-illuminated deep-depletion charge coupled device (CCD) camera operating at −60°C. Raman imaging measurements of cells were scanned in a raster pattern in the x–y plane with a constant stage speed and collecting a full Raman spectrum at speed of 0.5 seconds per pixel and a pixel resolution of 500 nm.

Immunofluorescence staining and fluorescence Microscopy

After treatment of cells with neratinib, lysosomes staining was employed using 75 nM of LysoTracker Red (DND-99; ThermoFisher GmbH, Dreieich, Germany) for 1h at 37°C, followed by cell fixation using 3.5% paraformaldehyde and fluorescence imaging was performed afterwards. Then, photo-bleaching of Lysotracker was achieved using white light for 15 min before proceeding for Raman measurements. After Raman measurements of cells grown on CaF_2 windows, the formalin-fixed cells were permeabilized with 0.2% Triton X-100 for 5 min at room temperature, washed with PBS, and blocked with 1% bovine serum albumin (BSA) for 30 min. Cells were incubated with the primary rabbit monoclonal anti-EGFR (ab30; Abcam, Cambridge, UK) and primary mouse monoclonal anti-HER2 (ab8054); Abcam, Cambridge, UK) overnight at 4°C, followed by washing with PBS buffer and incubation for 1 h at room temperature with fluorescein- (FITC; Jackson ImmunoResearch, West Grove, USA) and rhodamine (TRITC; Jackson ImmunoResearch, West Grove, USA) conjugated secondary antibodies, respectively. Excess antibodies were removed by washing several times with PBS. Cells were further incubated with 1,5-bis{[2-(dimethylamino)ethyl]amino}-4,8-dihydroxyanthracene-9,10-dione (DRAQ-5; Cell Signaling

Technology, Danvers, USA) for 10 min. Then, cells were washed with PBS. Similar experiments were performed without adding the LysoTracker Red staining using exactly the above protocol to make sure that Lysotracker staining has no effect on the Raman measurements.

Fluorescence measurements were performed with a confocal microscope (Leica TCS SP5 II) using a Leica HCX PL APO (25×/0.95 NA) water-immersion objective. The fluorescence imaging of lysosomes was performed using 561 nm excitation laser. Nuclear fluorescence was imaged by exciting with the 633 nm laser, whereas the fluorescence of HER2 and EGFR was imaged using the 488 and 561 nm excitation lasers, respectively.

Reaction of neratinib with lipids.

To prepare the stock solutions of lipids, 25 mg of 1,2-dipalmitoyl-sn-glycero-3-phosphocholine, (DPPC, Avanti), 1-palmitoyl-2-oleoyl-sn-glycero-3-phosphocholine (POPC, Avanti), and sodium salt of 1,2-dioleoyl-sn-glycero-3-phospho-L-serine (DOPS, Avanti) were dissolved in 1 mL chloroform. Mixtures of 10% DOPS with either POPC or DPPC stock solutions were prepared. Then, 25µl of each stock solutions were evaporated at RT under nitrogen gas. After the lipids were dried by a vacuum pump for 1h, they were dissolved in 100µl PBS buffer and vortexed for 1h at 37°C. 10µl of each lipid solution was added on CaF_2 slide and left to dry at room temperature. After it was completely dried, 10µl of neratinib was added to each lipid. The dried mixture of lipid and neratinib was measured by Raman micro-spectroscopy.

Reaction of neratinib with glutathione.

The reactivity of neratinib towards glutathione (GSH) was studied as described previously.[3] An aliquot of 100 mM stock solution of GSH (pH 7.0) was added to potassium phosphate buffer (pH 7.4) to prepare an incubation solution of 2 mM GSH. 3 mL of stock neratinib

solution (2 mM) in 100% DMSO was added to 600 mL buffer at a final concentration of 10 µM for pre-incubation for 5 min. The resultant mixture was incubated at 37°C for 30 min with shaking at 120 rpm. The product was measured by Raman micro-spectroscopy.

Liquid chromatography-mass spectrometry

Identification of the neratinib metabolites was performed by LC-MS analytics. After treatment of cells with neratinib and fixation, an NE-PER kit (ThermoFisher GmbH, Dreieich, Germany) was employed to extract the nuclear and cytoplasmic content of cells, which can be utilized in LC-MS analysis. Data were obtained from a Shimadzu LCMS-8030 triple quadrupole mass spectrometer, equipped with an electrospray source and an SPD-M20A diode array detector and using a C18 reversed-phase column (Phenomenex Kinetex, 2.6 µm, 100A, 100×2.1 mm) including a C18 guard column (Phenomenex SecurityGuard ULTRA). Mobile phases A and B consisted of water containing 0.1% formic acid (v/v) and methanol containing 0.1% formic acid (v/v), respectively. All mobile phase solvents and additives were of LC-MS grade (VWR HiPerSolv Chromanorm). After injecting 8 µL of sample, the analytes were eluted with the following gradient method at 40 °C and a flow rate of 0.5 mL/min: 0-0.2 min 10% B, 0.3-3.0 min 70% B, 3.1-3.5 min 98% B, 3.7-6.0 min 10% B. Analytes were detected sequentially in the DAD detector (detection range 200-600 nm) and by ESI-MS analysis. The following standard instrument parameters were used: Nebulizing gas flow 3 L/min, dilution line temperature 250°C, heat block temperature 400°C, drying gas flow 15 L/min, CID gas 230 kPa, ion gauge vacuum 1.7·10-3 Pa, Interface voltage 4.5 kV. Mass detection (set to the maximum possible scan speed of 15000 u/s for each experiment) occurred after positive electrospray ionization in scan mode (scan ranges (+): m/z = 50-205 and 200-700) for both detector quadrupoles from 0-5 min and in single ion mode (SIM+/Q3) set to m/z values of the $[M+H]^+$ and $[M]^+$ ions of neratinib and the expected metabolite structure from 0-2.5 min. For product ion scan (PIS) experiments, either the

molecular ions $[M+H]^+$ or the $[M]^+$ of the desired compound was isolated (Q1) and fragmentation induced at different collision energies of -2 V, and -5 to -40 V in 5 V-steps. The resulting fragments were detected in ranges of m/z = (+/Q3) 50-205 and 200-700 and investigated individually for each collision energy as well as considered as an overlay.

The experiments proceeded in the following way: First, pure scan (scan range m/z (+/-) 200-700 in both detector quadrupoles) alongside with SIM+ experiments for neratinib ($[M+H]^+$ at m/z = 557.2) were carried out for chromatographic method development and identification of potential metabolite masses. Based on these data, scan/SIM+ experiments were carried out to confirm pre-identified potential candidates. Combined with the Raman results, three metabolite masses were identified from these data sets. Their potential structure was elucidated with targeted SIM/PIS experiments as described above. Table S1, as well as Figures S31-S34, give an overview of the isolated masses and diagnostic fragment peaks.

Relevant fragment data for neratinib metabolites was solely found in the cytosol fractions of the cellular samples. Even though signals for the mass of free neratinib were observed in the nucleus fraction as well, no characteristic fragmentation patterns were obtained. Data analysis was therefore focused on the cytosolic fractions. All isolated fragments gave peaks of lower intensity compared with free neratinib, indicating a lower abundance and a significant amount of non-metabolized drug within the samples. These results are in good accordance with those obtained from the Raman spectroscopic experiments.

In the PIS experiments, the most meaningful fragment peak observed for all metabolite masses was the signal belonging to a putative $[M-2]^+$ resp. $[M+H-2]^+$ fragment, depending on the precursor ion (Table S1, Figures S16-S19). Such a fragment most probably originates from an *in situ* ring closure reaction upon formal abstraction of H_2, likely based on the presence of a hydroxy- or keto group next to the cyano function in metabolites **I**, **IIa/b** and **IIIa/b** (Scheme S1). A comparable fragment peak was not observed for intact neratinib.

Fragment peaks in the lower *m/z* range (*m/z* < 200) were not assigned unambiguously. The observed peaks were, however, generally characteristic for each mother peak and re-occurred in the different cell lines (Table S1), thus confirming their structural similarity.

Multivariate Analysis

The Raman spectra of cells were analyzed using multivariate analysis such as HCA. Raman hyperspectral results were imported into MATLAB 8.2 (MathWorks Inc., MA), and data pre-processing and cluster analyses were performed using in-house built scripts. Cosmic spikes were removed using an impulse noise filter, and Raman spectra were interpolated to a reference wavenumber scale. All spectra were then baseline-corrected using a third-order polynomial function and were vector normalized. We performed HCA on the regions of 700—1800 and 2100—2280 cm^{-1} using Ward's clustering in combination with the Pearson correlation distance.

Quantum chemical calculations

Calculations were conducted using the gaussian03 program package. The geometry of the fragments shown in Scheme 1 was optimized at the B3LYP/6-31G(d) level of theory. All vibrational frequencies were calculated analytically. Furthermore, the polarizability derivatives were used to acquire the non-resonant Raman intensities. The scaling factor in this calculation was 0.960. We have also performed DFT calculations for different neratinib conformers and show here only the results of the lowest energy conformers.

Table S1. Diagnostic fragment peaks of neratinib and the three identified metabolite masses as found in the cytosol fraction of the respective cells. *m/z* Values are given as the average of generally at least 3 observed peaks from individual collision energies, only in cases of broad distribution, observed ranges are given.

Cpd / met.	**Mono-isotopic mass**	**Precursor [*m/z*]**	**Diagnostic fragment peaks [*m/z*]**			**Precursor [*m/z*]**	**Diagnostic fragment peaks [*m/z*]**		
			NCI-H1975	**Calu-3**	**SK-BR-3**		**NCI-H1975**	**Calu-3**	**SK-BR-3**
I	449.09	449.10	n.d.*	n.d.	57	450.10	55	55	
							77	77	
					80				
					83			84	
							86	86	85
							99	99	99
					129		129	129	129
					174		174	174	174
							196	196	
					198				
			n.d.	n.d.	447		n.d.	448	448
II a/b/c	433.09	433.10	55	55	57	434.10	55	55	n.d.
			85	85	83-86		85	86	
			89.8	89.8			89 90	90	
			109	109	106-107		107-109	108-109	
			127	127-128	126-127		127 129	127 129	
			130.8	130	129		132	131	
			141	141	141		142		
			174	174	173		174		
			431	n.d.	431		n.d.	n.d.	n.d.
III a/b/c	461.13	461.15	63 70	63 70	63 67 69-70	462.15	63 70	64 70	n.d.
			86	86	86		86	86 89	
			113		113			108	
			130	130	130		130	130	
			141	141	141		141	141	
			163	163	163		163	163	
			172 174	174			174	174	
			185	185	185		185	185	
			459	459	459		n.d.	n.d.	460
Neratinib	556.20					557.20**		69	
								82	
								84	
								93	
								94	
								112	
								556.7	

* n.d. – no data extractable.

** Reference data was obtained from pure Neratinib injected without cellular matrix.

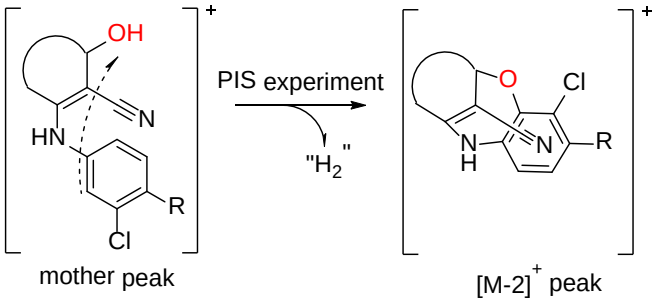

Scheme S1. Potential *in situ* ring closure reaction of neratinib metabolites I, IIa/b or IIIa/b during PIS experiments.

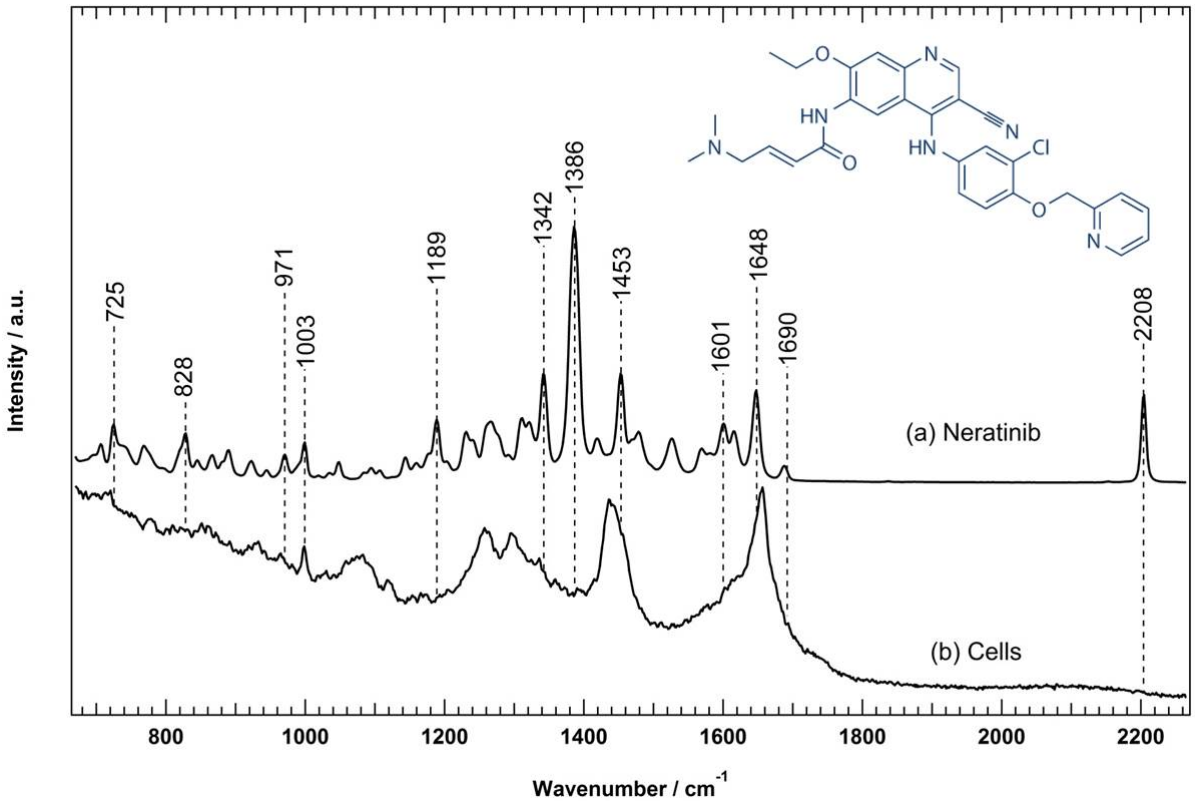

Figure S1. Raman spectra of free neratinib (a) and untreated SK-BR-3 cells (b, control). The chemical structure of neratinib is also shown.

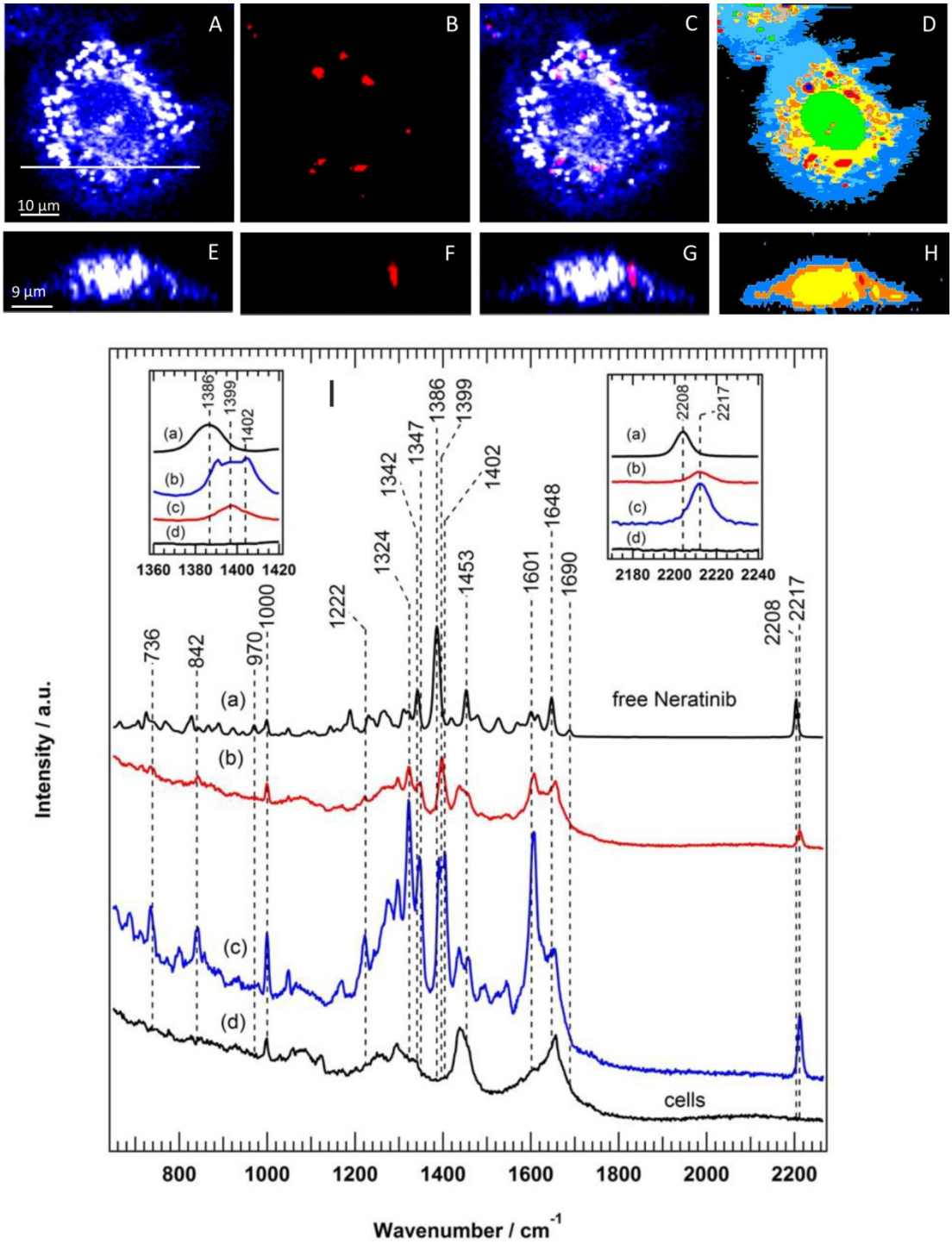

Figure S2. Raman imaging of NSCLC NCI-H1975 cell treated with 5 µM neratinib for 8 h. Raman images reconstructed from the (A) C—H deformation (1425—1470 cm^{-1}) and (B) C≡N stretching (2200—2225 cm^{-1}) intensities. (C) Overlay of Panels A and B. (D) HCA results based on the Raman data shown in Panel A. (E-G) Cross-section Raman images along the x, z-direction of the same cell. Scanning positions are indicated by the white line in Panel A. (H) HCA results based on the Raman data shown in Panel E. (I) Raman spectrum of free neratinib (a), the average Raman spectra of drug regions within the cell of the red (b) and blue (c) clusters in Panel D, and Raman spectrum of untreated cells (d, control) are shown. The insets show enlarged spectra around the characteristic 1386 and 2208 cm^{-1} bands.

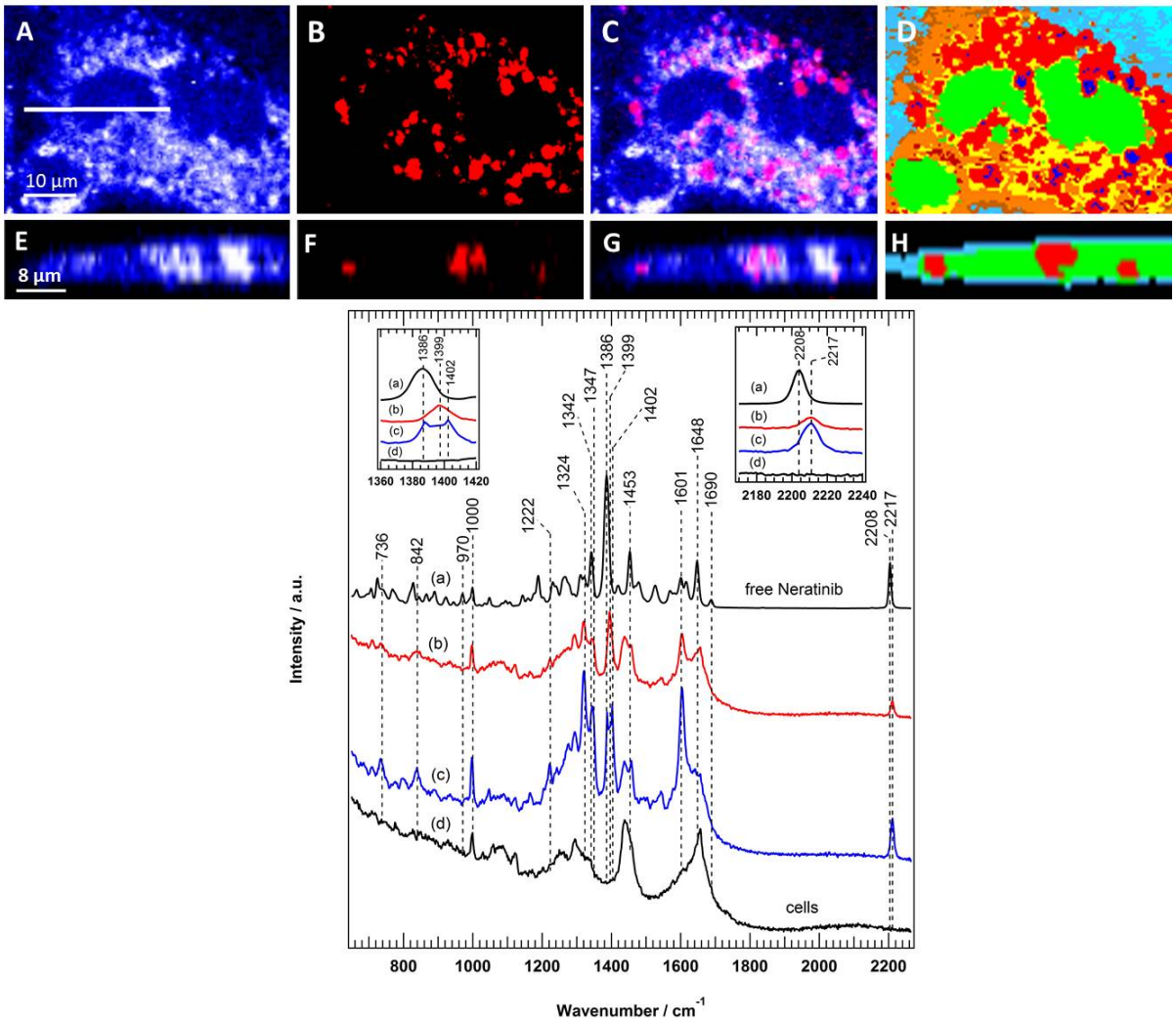

Figure S3. Raman imaging of NSCLC Calu-3 cells treated with 5 µM neratinib for 8 h. Raman images reconstructed from the (A) C—H deformation (1425—1470 cm^{-1}) and (B) C≡N stretching (2200—2225 cm^{-1}) intensities. (C) Overlay of Panels A and B. (D) HCA results based on the Raman data shown in Panel A. (E-G) Cross-section Raman images along the x, z-direction of the same cells. Scanning positions are indicated by the white line in Panel A. (H) HCA results based on the Raman data shown in Panel E. (I) Raman spectrum of free neratinib (a), the average Raman spectra of drug regions within cells of the red (b) and blue (c) clusters in Panel D, and Raman spectrum of untreated cells (d, control) are shown. The insets show enlarged spectra around the characteristic 1386 and 2208 cm^{-1} bands.

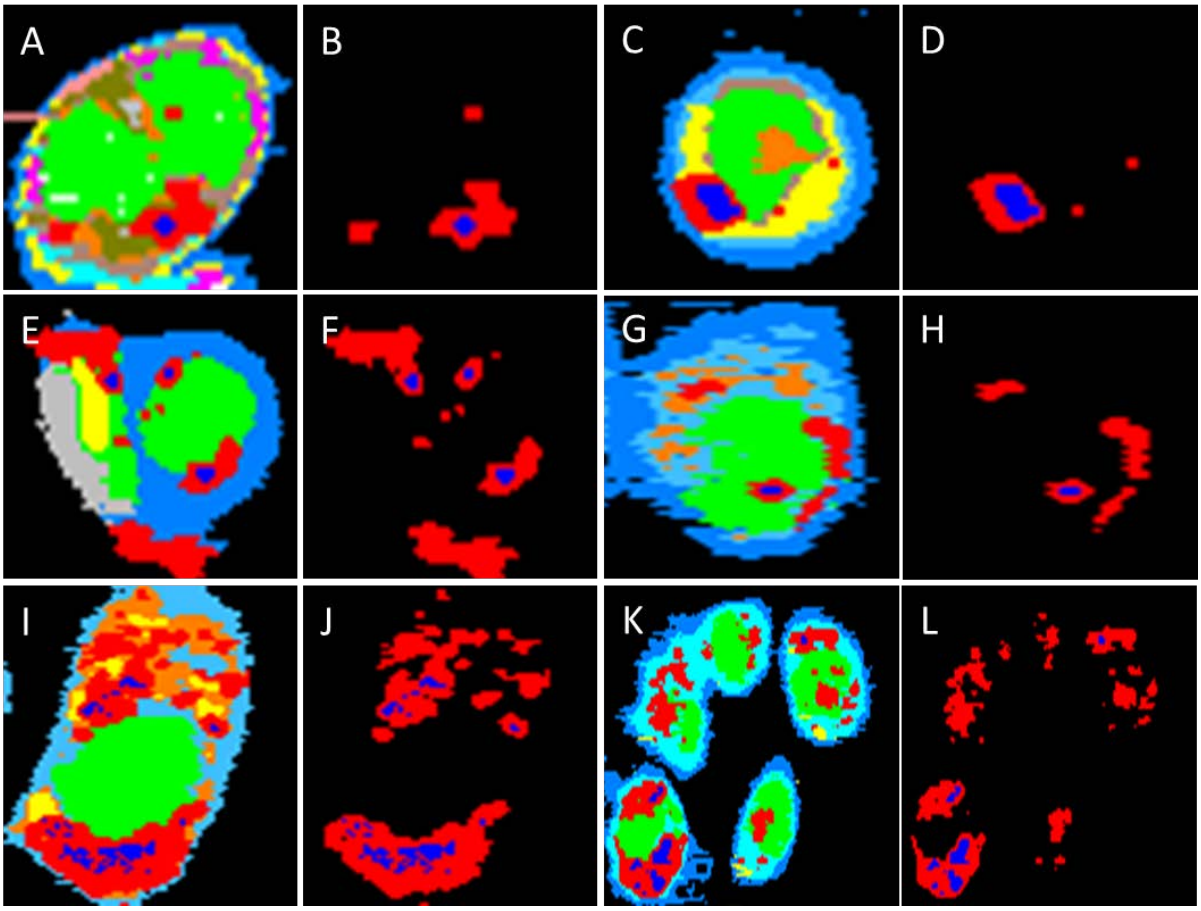

Figure S4. (A,C,E,G,I,K) HCA index-color images of the Raman results of several replicates of SK-BR-3 cells treated with 5 µM neratinib and (B,D,F,H,J,L) their corresponding drug-containing clusters (M1: red and M2: blue).

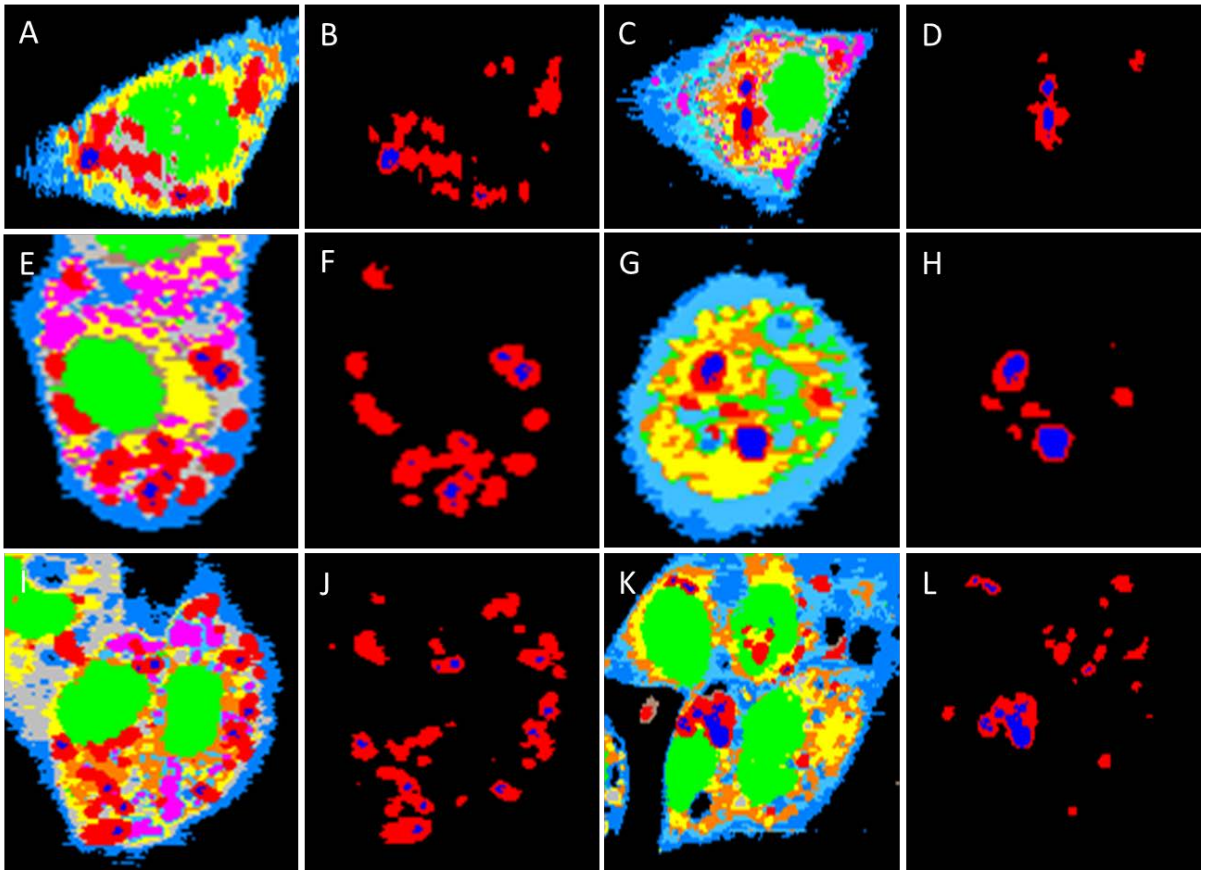

Figure S5. (A,C,E,G,I,K) HCA index-color images of the Raman results of several replicates of NCI-H1975 cells treated with 5 µM neratinib and (B,D,F,H,J,L) their corresponding drug-containing clusters (M1: red and M2: blue).

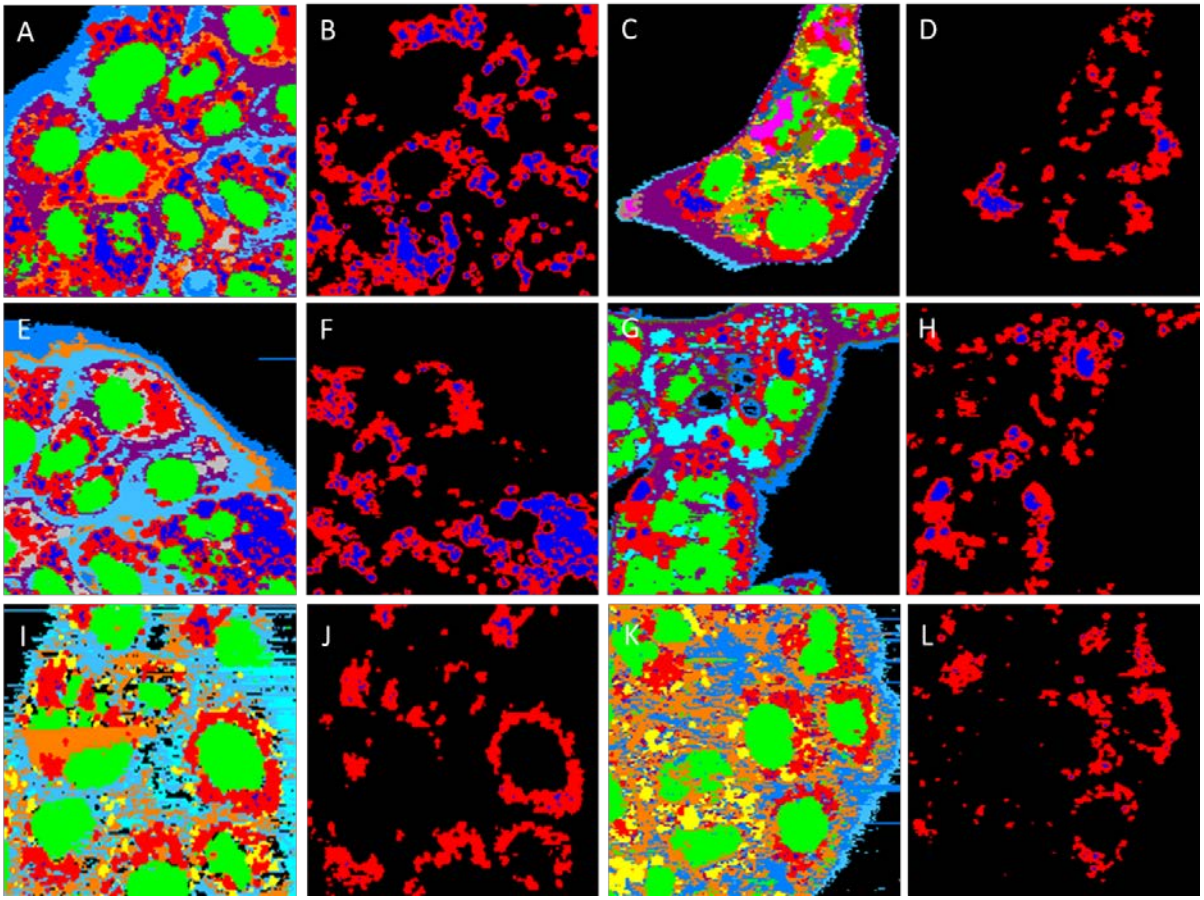

Figure S6. (A,C,E,G,I,K) HCA index-color images of the Raman results of several replicates of Calu-3 cells treated with 5 µM neratinib and (B,D,F,H,J,L) their corresponding drug-containing clusters (M1: red and M2: blue).

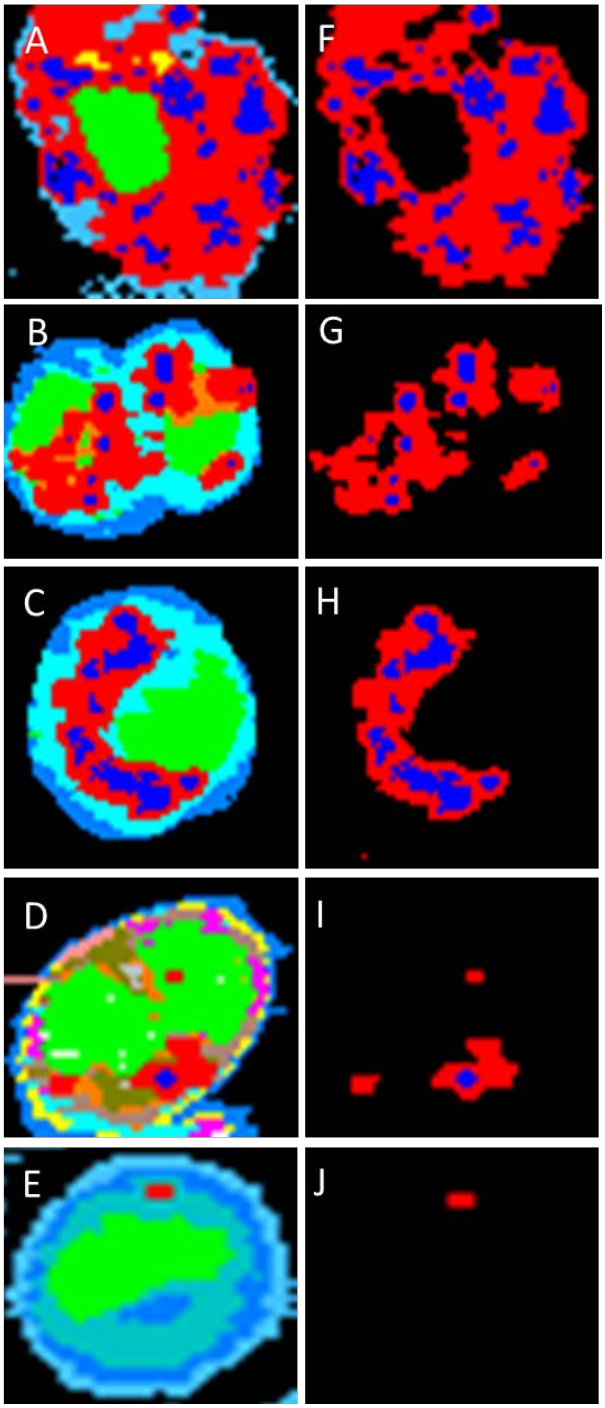

Figure S7. (A-E) HCA index-color images of the Raman results of concentration dependence measurements in which SK-BR-3 cells treated with 50 µM (A), 25 µM (B), 10 µM (c), 5 µM (d), and 1 µM (E) neratinib and (F-J) their corresponding drug-containing clusters (M1: red and M2: blue).

We have optimized our Raman experiments to detect low neratinib concentration in cells. First, we have performed concentration dependence experiments for each cell-line (Figures S7-S9) in which cells were treated with different neratinib concentrations (50-0.5 µM). The cellular uptake was very efficient and dependent on the neratinib concentration. The cellular uptake was massive when cells were treated with high neratinib concentration (Panels A and

B, 50 μM). As the concentration of neratinib decreased (Panels B-E and G-J), the cellular uptake was also reduced as expected and reasonable intracellular neratinib was detected, implying that neratinib binds specifically to the receptors. Second, we have performed several replicates of these measurements as shown in Figures S4-S6 and S18-S26 to confirm the reproducibility of the Raman imaging results.

Under our current experimental conditions, cellular uptake was very efficient, which leads to an increase in the intracellular local concentration of neratinib as indicated also in Figure S17. This higher local intracellular neratinib concentration (6.2-9.6 (±1.0-1.2) mM) is most likely the main reason for the stronger neratinib Raman signal when cells treated with low neratinib concentrations.

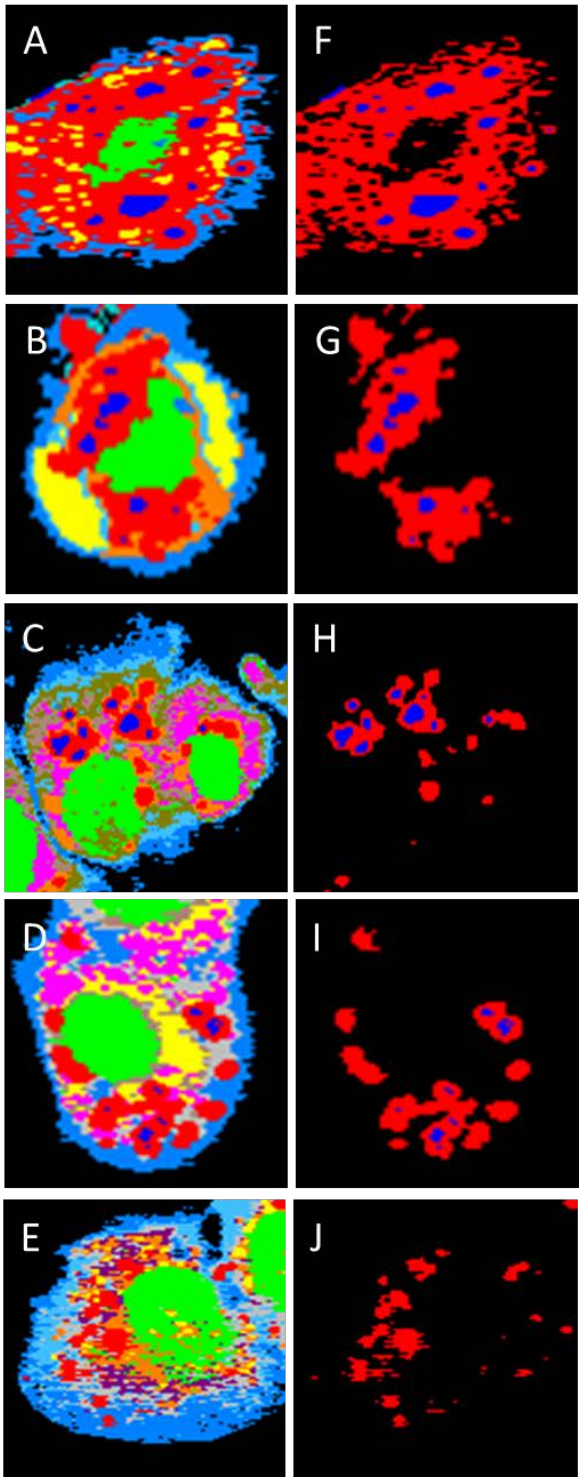

Figure S8. (A-E) HCA index-color images of the Raman results of concentration dependence measurements in which NCI-H1975 cells treated with 50 μM (A), 25 μM (B), 10 μM (c), 5 μM (d), and 1 μM (E) neratinib and (F-J) their corresponding drug-containing clusters (M1: red and M2: blue).

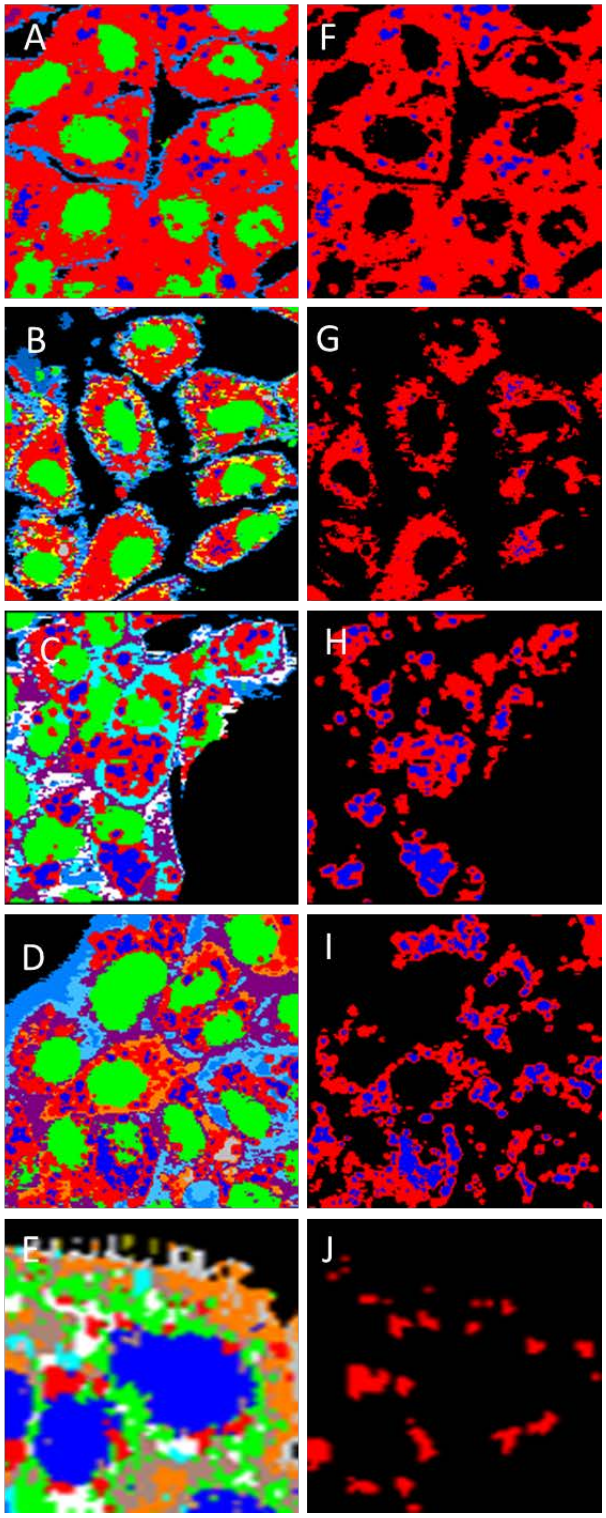

Figure S9. (A-E) HCA index-color images of the Raman results of concentration dependence measurements in which Calu-3 cells treated with 50 µM (A), 25 µM (B), 10 µM (c), 5 µM (d), and 1 µM (E) neratinib and (F-J) their corresponding drug-containing clusters (M1: red and M2: blue).

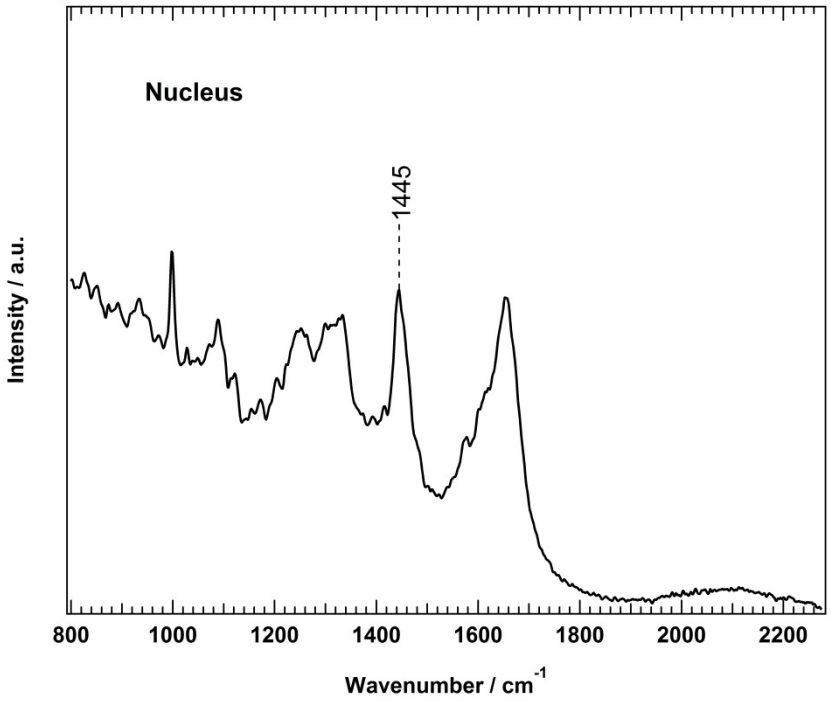

Figure S10. Average Raman spectrum of the nucleus of SK-BR-3 cells of the green cluster of HCA result shown in Figure 1D. Based on the nucleus staining of the same cell (Figure 3B), the green cluster was assigned to the nucleus.

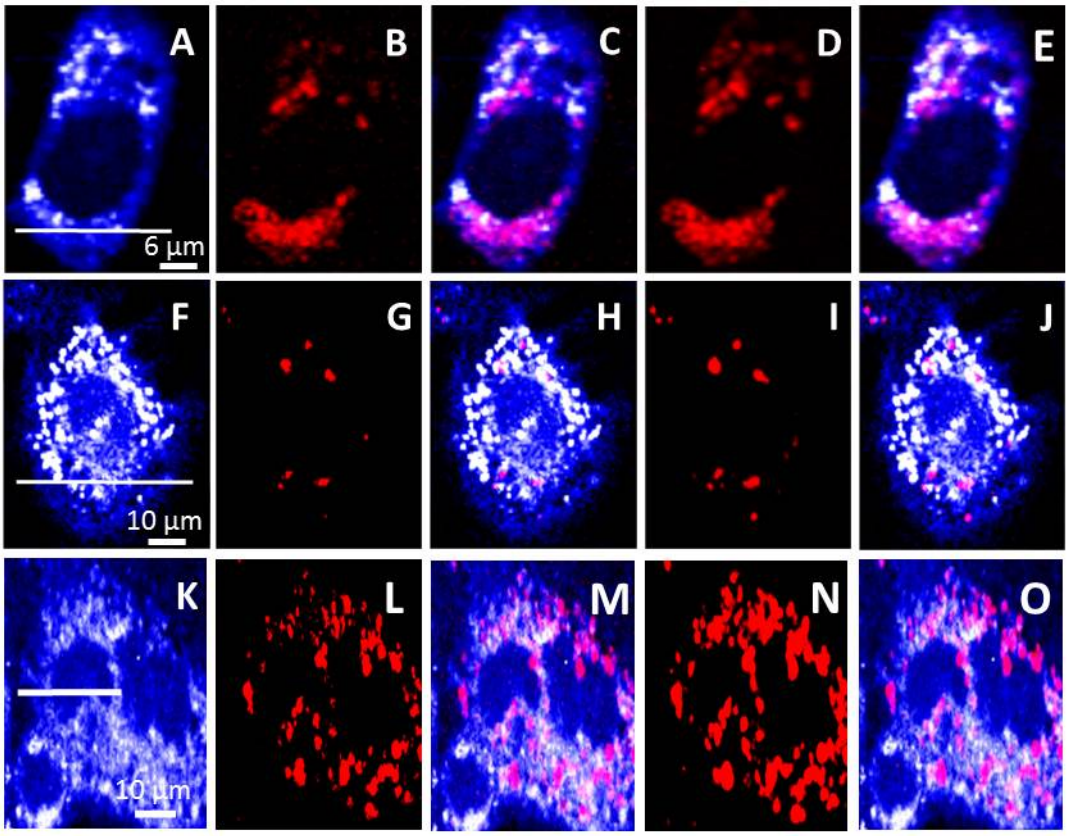

Figure S11. Raman imaging of SK-BR-3 (A-E), NCI-H1975 (F-J), and Calu-3 (K-O) treated with 5 µM neratinib for 8 h. Raman images reconstructed from the 1425—1470 cm^{-1} (A,F,K), the 2200—2225 cm^{-1} (B,G,L), and the 1380—1410 cm^{-1} (D,I,N) band intensities. The overlay of (A,F,K) with either (B,G,L) or (D,I,N) is shown in (C,H,M) and (E,J,O), respectively.

Neratinib has a strong Raman band at 1386 cm^{-1} in the fingerprint region (Figure 2a) that can also be used as a label-free marker for neratinib in cells. This is because the Raman spectrum of cells (Figure 2d) has no bands at this wavenumber position.

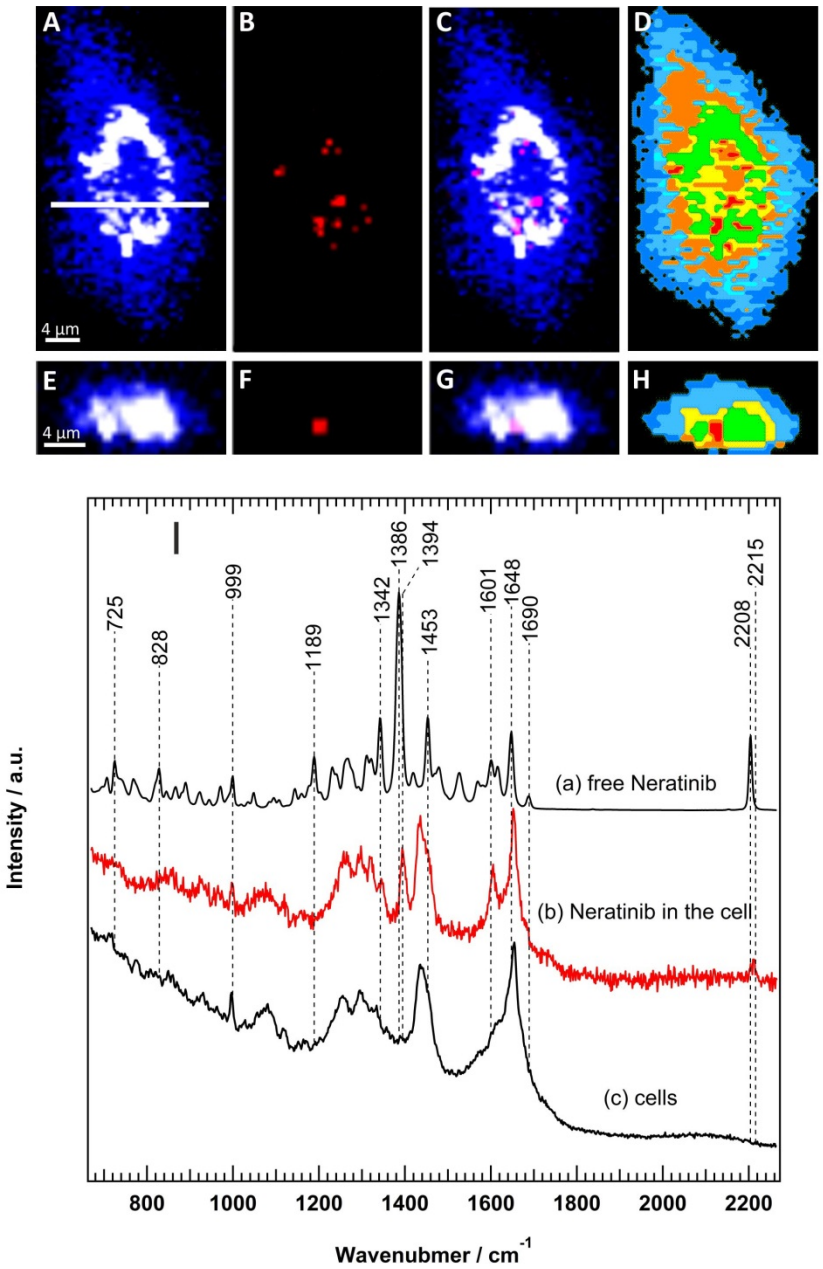

Figure S12. Raman imaging of NSCLC NCI-H1975 cell treated with low neratinib concentration (0.5 μM) for 8 h. Raman images reconstructed from the 1425—1470 cm^{-1} (A) and 1380—1410 cm^{-1} (B) band intensities. (C) Overlay of Panels A and B. (D) HCA results based on the Raman data shown in Panel A. (E-G) Cross-section Raman images along the x, z-direction of the same cell. Scanning positions are indicated by the white line in Panel A. (H) HCA results based on the Raman data are shown in Panel E. (I) Raman spectrum of free neratinib (a), the average Raman spectra of drug regions within the cell of the red cluster (b), and Raman spectrum of untreated cells (c, control) are shown.

When cells were treated with 5 μM neratinib, the Raman intensity of neratinib bands of for instance M1 in cells is decreased but the band at 1386 cm^{-1} band in addition to a weak band at 2208 cm^{-1} is clearly seen (Figures 2 and S2-S3). However, when the neratinib concentration is further reduced to 1-0.5 μM, the overall Raman signal of neratinib bands in cells is decreased (Figure S12) and only the 1386 cm^{-1} band is clearly distinguishable and the CN (2215 cm^{-1}) band is very weak and within the S/N ratio. Therefore, the 1386 cm^{-1} band can safely be used as a label-free marker to monitor the distribution of neratinib at low concentration.

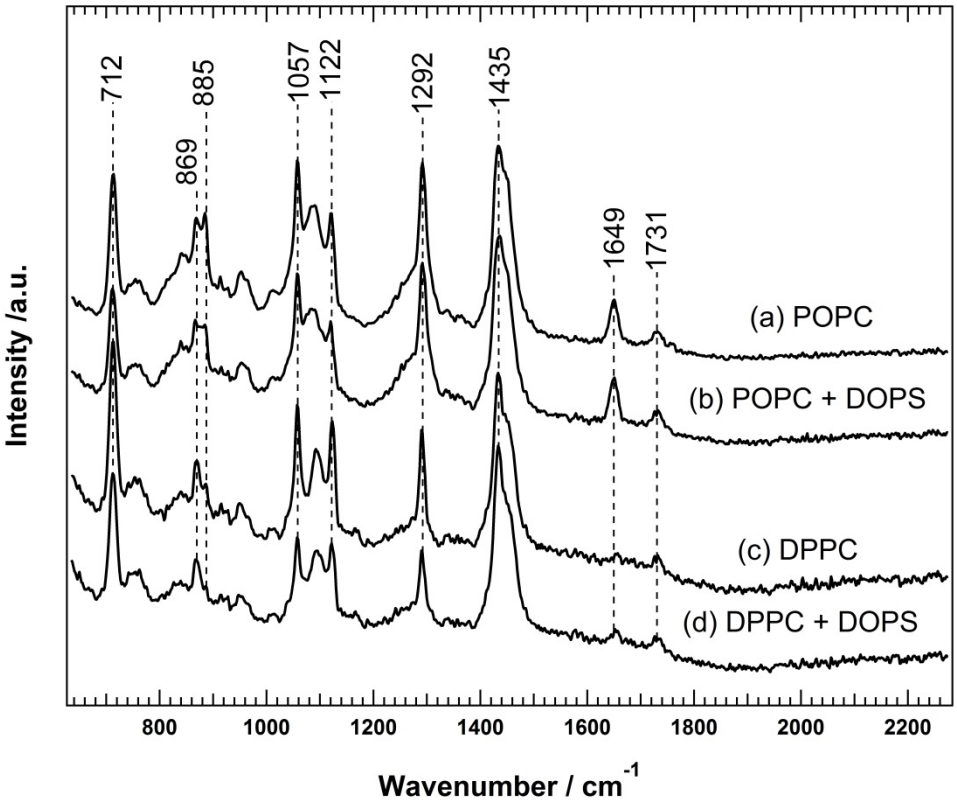

Figure S13. Raman spectra of (a) POPC, (b) POPC/DOPS, (c) DPPC, and (d) DPPC/DOPS lipids.

It is obvious that lipids have no contribution to the characteristics Raman bands of neratinib at 1386 and 2208 cm^{-1}.

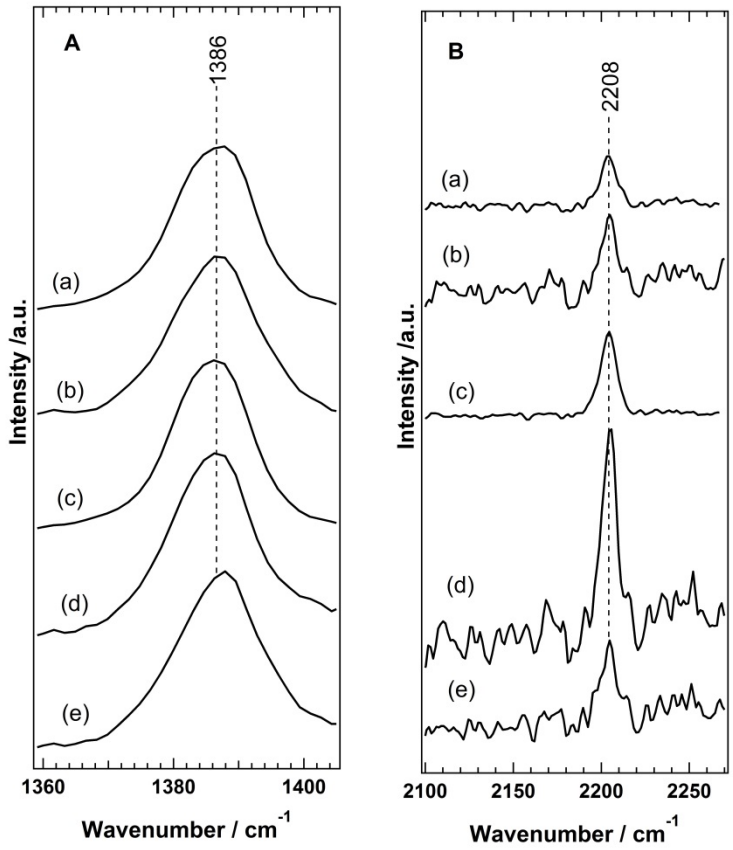

Figure S14. Raman spectra of (a) free-neratinib and neratinib attached to (b) POPC, (c) POPC/DOPS, (d) DPPC, and (e) DPPC/DOPS lipids.

We have performed Raman measurements in which neratinib attached to POPC, POPC/DOPS, DPPC, and DPPC/DOPS lipids to investigate the environmental effect of for instance lipids on neratinib. As shown in Figure S14 the Raman results indicate that the lipids did not produce a significant wavenumber shift of the 1386 and 2208 cm^{-1} Raman bands of neratinib but only change in the Raman intensity is observed. Therefore, we suggest that the observed Raman spectral changes including wavenumber shift of the Raman bands (1386 and 2208 cm^{-1}) of intracellular neratinib in Figure 2(b,c) are due to metabolism but not due to the environmental effect of for instance lipids.

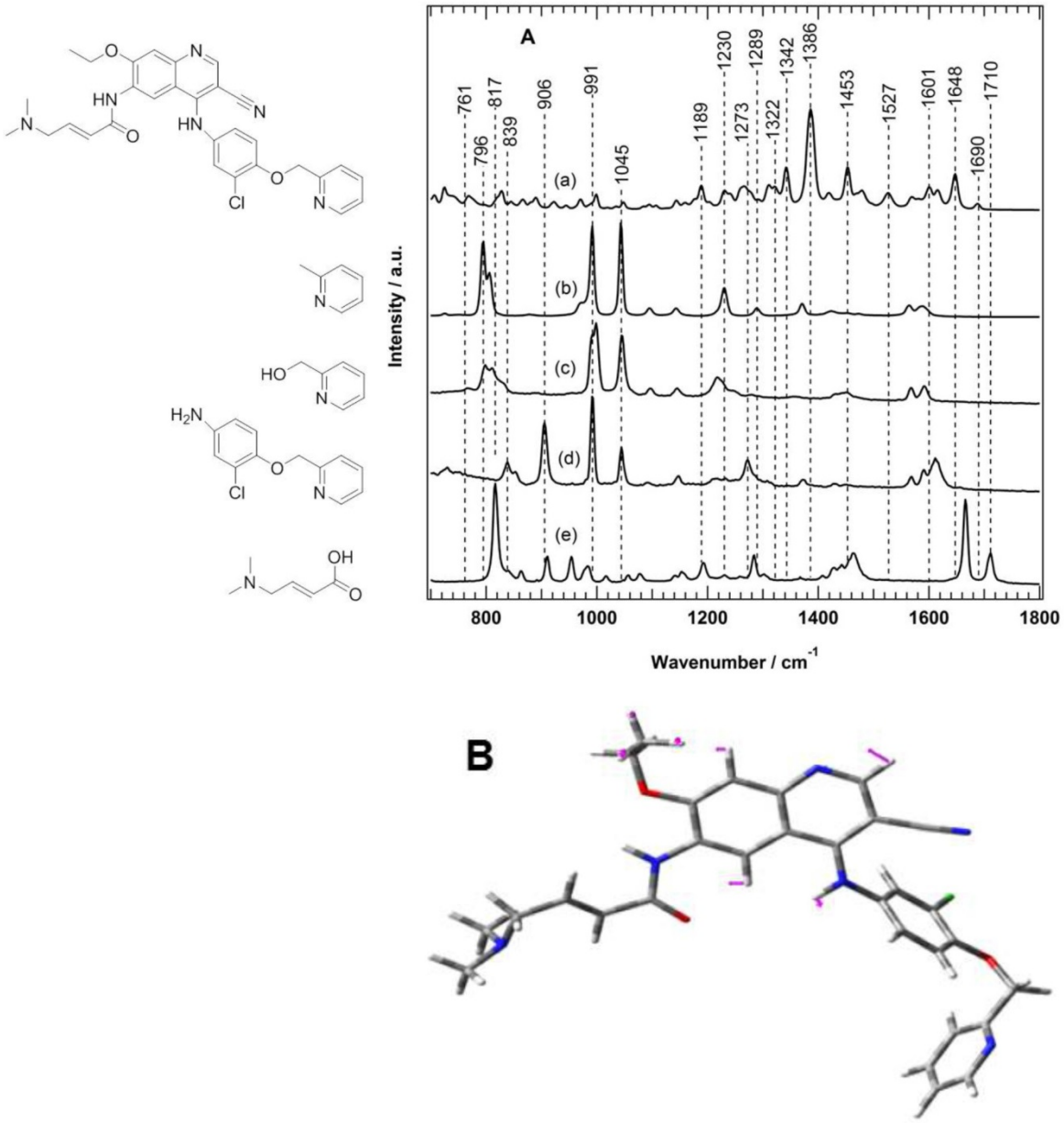

Figure S15. (A) Raman spectra of neratinib precursors. Raman spectra of free neratinib (a), 2-methylpyridine (b), pyridine-2-methanol (c), 3-chloro-4-(2-pyridinylmethoxy) aniline (d), and dimethylamino crotonic acid (e). The chemical structure of neratinib and its precursors are also displayed. (B) Atomic displacement vectors for the 1386 cm^{-1} vibration of neratinib.

The Raman band at 1386 cm^{-1} in the spectrum (a) of neratinib is absent in the spectra (b-e) suggesting that this band originates from quinoline ring of neratinib.

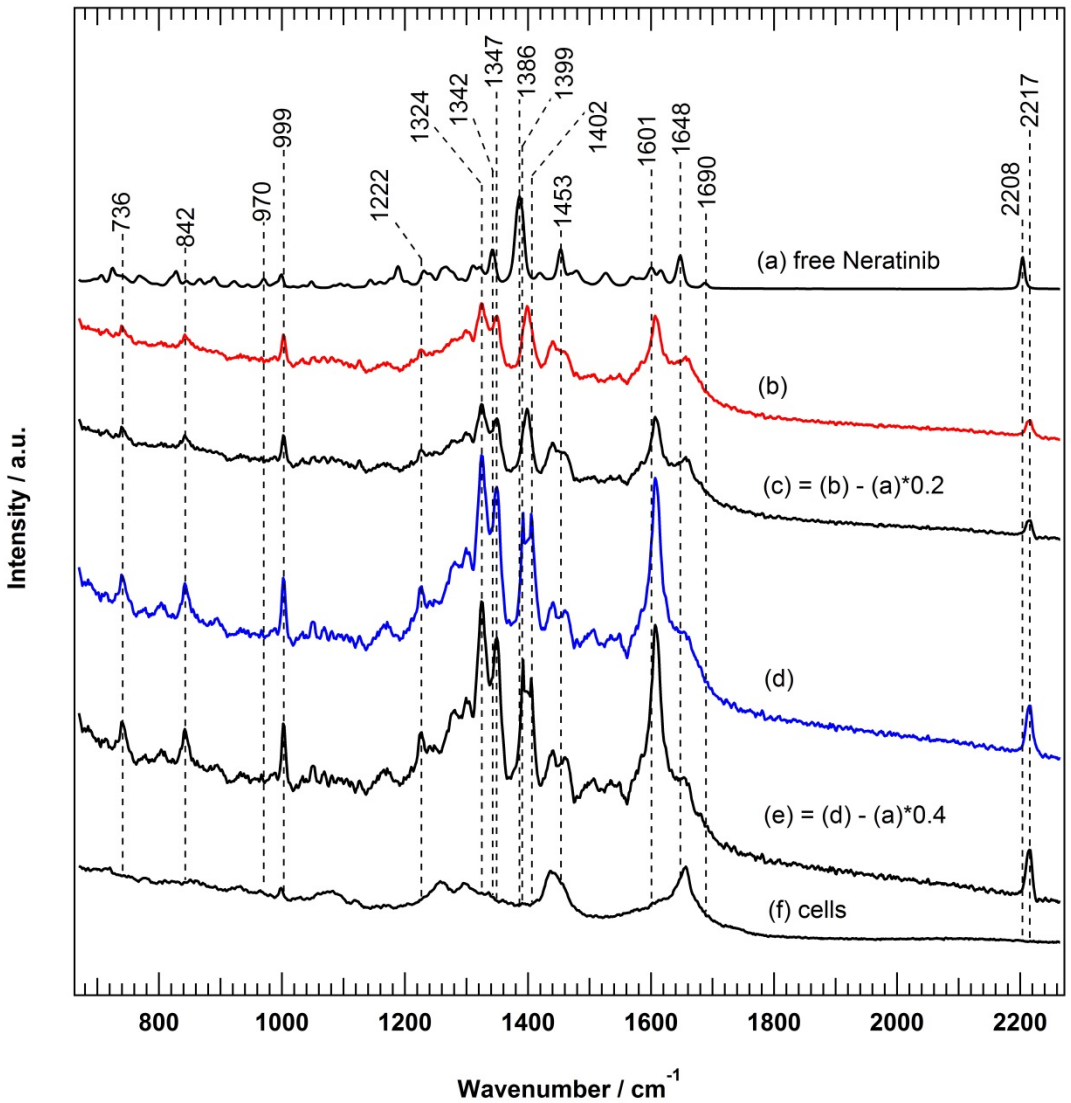

Figure S16. Raman spectrum of free neratinib (a), the average Raman spectra of drug regions within the cell of the red (b) and blue (d) clusters in (Figure 1D), and spectrum of untreated cells (f). Fractions of free neratinib (a) were subtracted from the spectra of (b) and (d) without obtaining negative bands and the results are shown in spectra (c) and (e), respectively.

Fractions of free neratinib were subtracted successfully from the spectra (b and d) of metabolites without obtaining negative bands in the difference spectra (c and e). These results suggest that free neratinib contributes to the spectra (b and d) of metabolites.

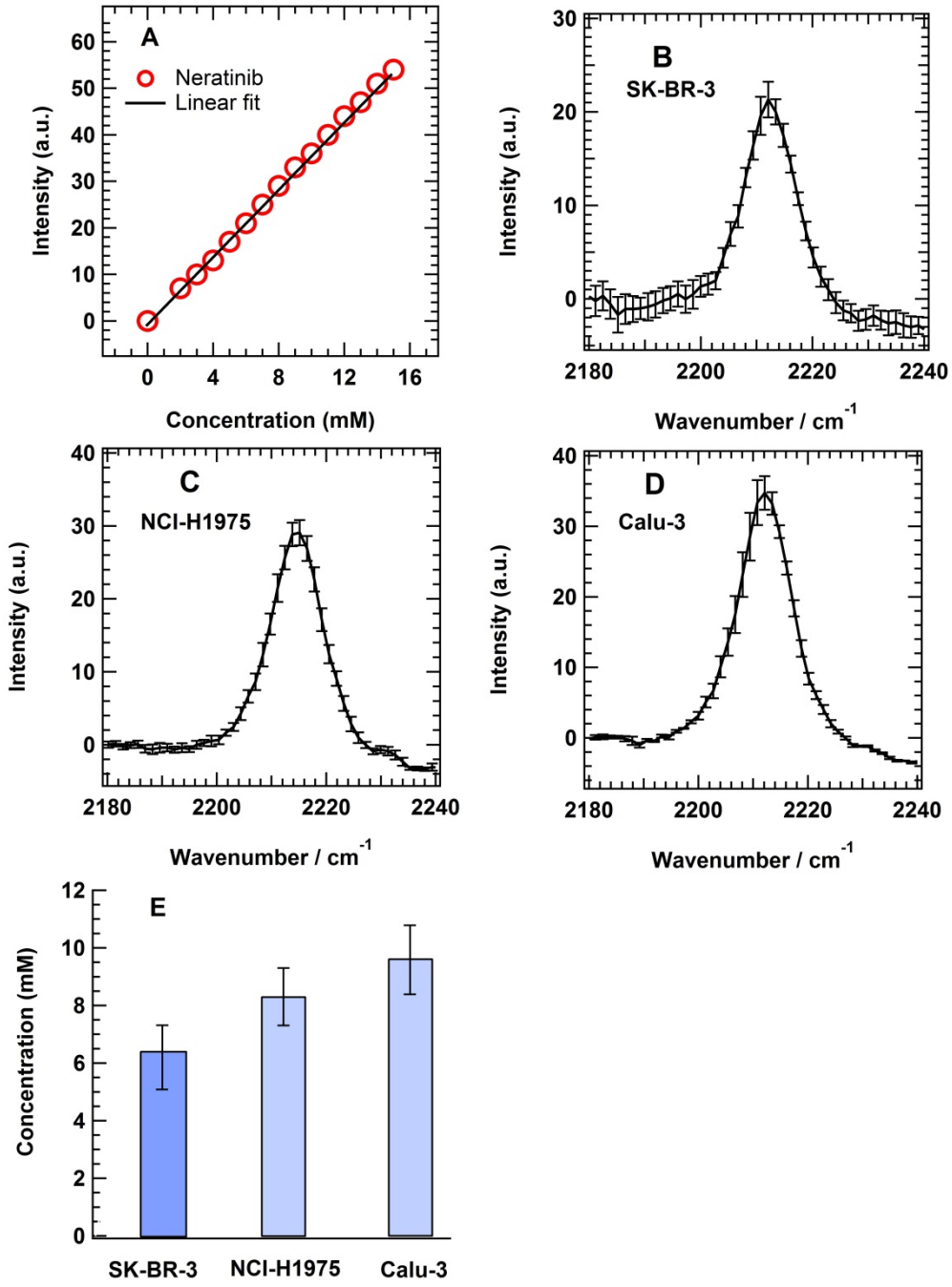

Figure S17. (A) A calibration curve depicting the Raman intensity of the C≡N band (2208 cm^{-1}) of neratinib (dissolved in DMSO) of known concentrations. The average Raman spectra of neratinib in cells of at least five of (B) SK-BR-3 cells, (C) NCI-H1975 cells, and (D) Calu-3 cells. (E) The calculated concentration of neratinib in different cancer cells. Error bar shows standard deviation.

Neratinib Raman bands below 2 mM were not detected. The calculated neratinib concentration within cancer cells is 6.2 (±1.1) mM in SK-BR-3 cells, 8.3 (±1.0) mM in NCI-H1975 cells, and 9.6 (± 1.2) mM in Calu-3 cells, which are 1240 (±220), 1660 (±200), and 1920 (±240) folds, respectively, higher than the neratinib extracellular concentration (5 μM). Such high intracellular drug concentration was also reported for other TKIs such as imatinib and nilotinib.[4] It is noted that we could not use the strong Raman band of neratinib at 1386 cm^{-1} in the calibration curve because it overlaps with a Raman band of DMSO.

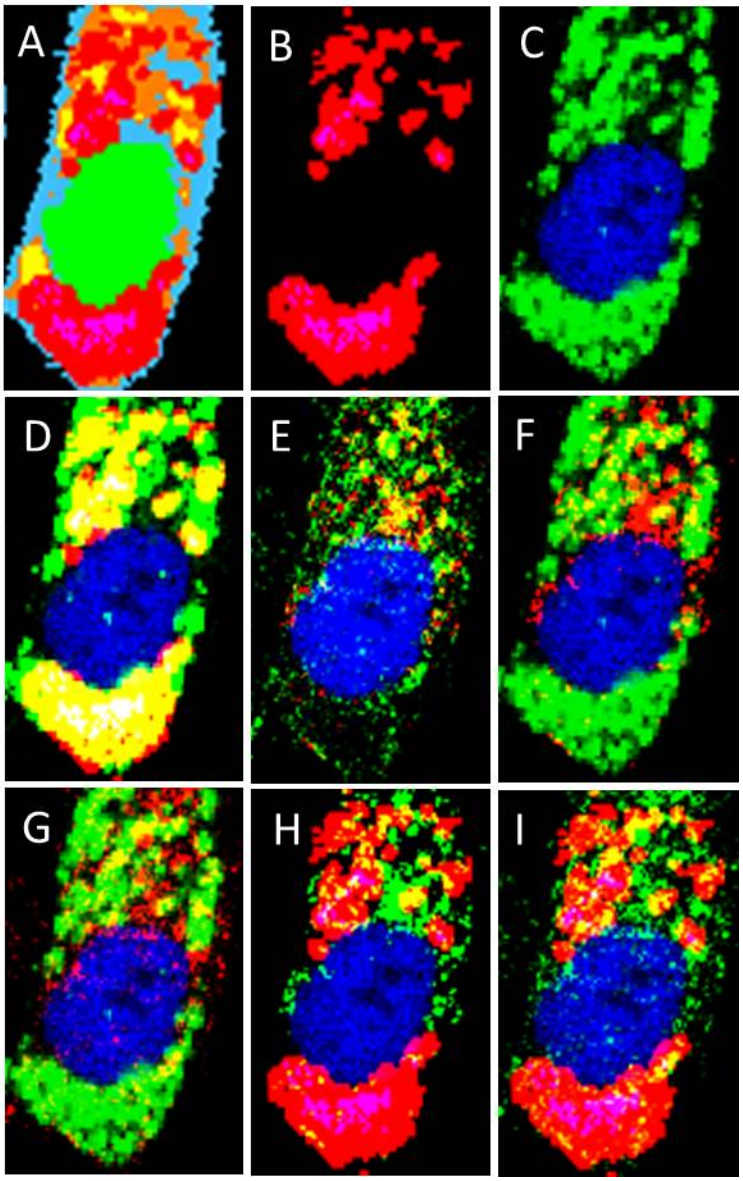

Figure S18. Raman and fluorescence imaging of SK-BR-3 cell treated with 5 μM neratinib for 8h. (A) HCA of the Raman results of the cell. (B) HCA of neratinib-containing clusters in the cell, (C) fluorescence image of the same cell that shows lysosomes (green) surrounding the nucleus (blue), and (D) an overlay (yellow and white) of (B) and (C). (E) Fluorescence image of the same cell that shows EGFR (red) and HER2 (green) distribution around the nucleus. An overlay (yellow) of (C) with EGFR (red) and HER2 (red) is shown in Panels (F) and (G), respectively. An overlay (yellow and white) of (B) with EGFR (green) and HER2 (green) is also shown in Panels (H) and (I), respectively. Part of this Figure is shown in Figure 3.

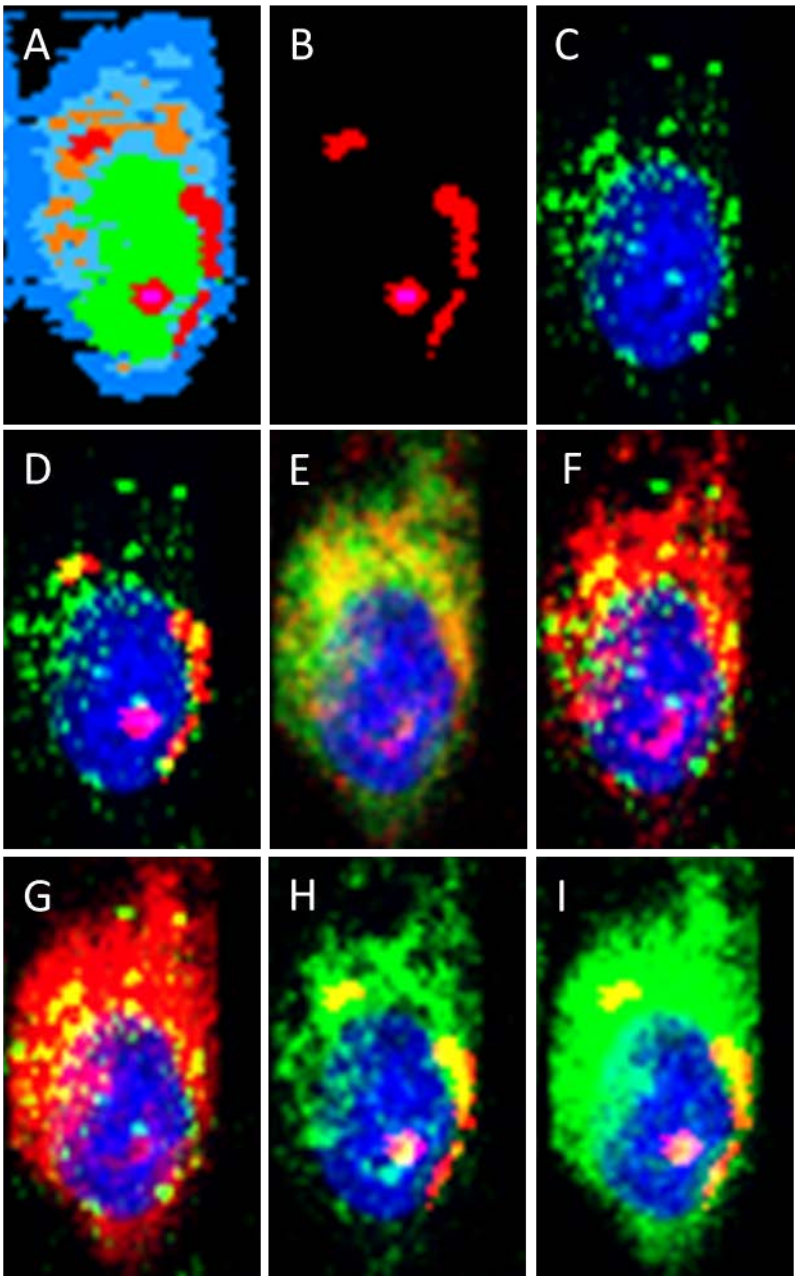

Figure S19. Raman and fluorescence imaging of SK-BR-3 cell treated with 5 μM neratinib for 8h. (A) HCA of the Raman results of the cell. (B) HCA of neratinib-containing clusters in cell, (C) fluorescence image of the same cell that shows lysosomes (green) surrounding the nucleus (blue), and (D) an overlay (yellow and white) of (B) and (C). (E) Fluorescence image of the same cell that shows EGFR (red) and HER2 (green) distribution around the nucleus. An overlay (yellow) of (C) with EGFR (red) and HER2 (red) is shown in Panels (F) and (G), respectively. An overlay (yellow and white) of (B) with EGFR (green) and HER2 (green) is also shown in Panels (H) and (I), respectively.

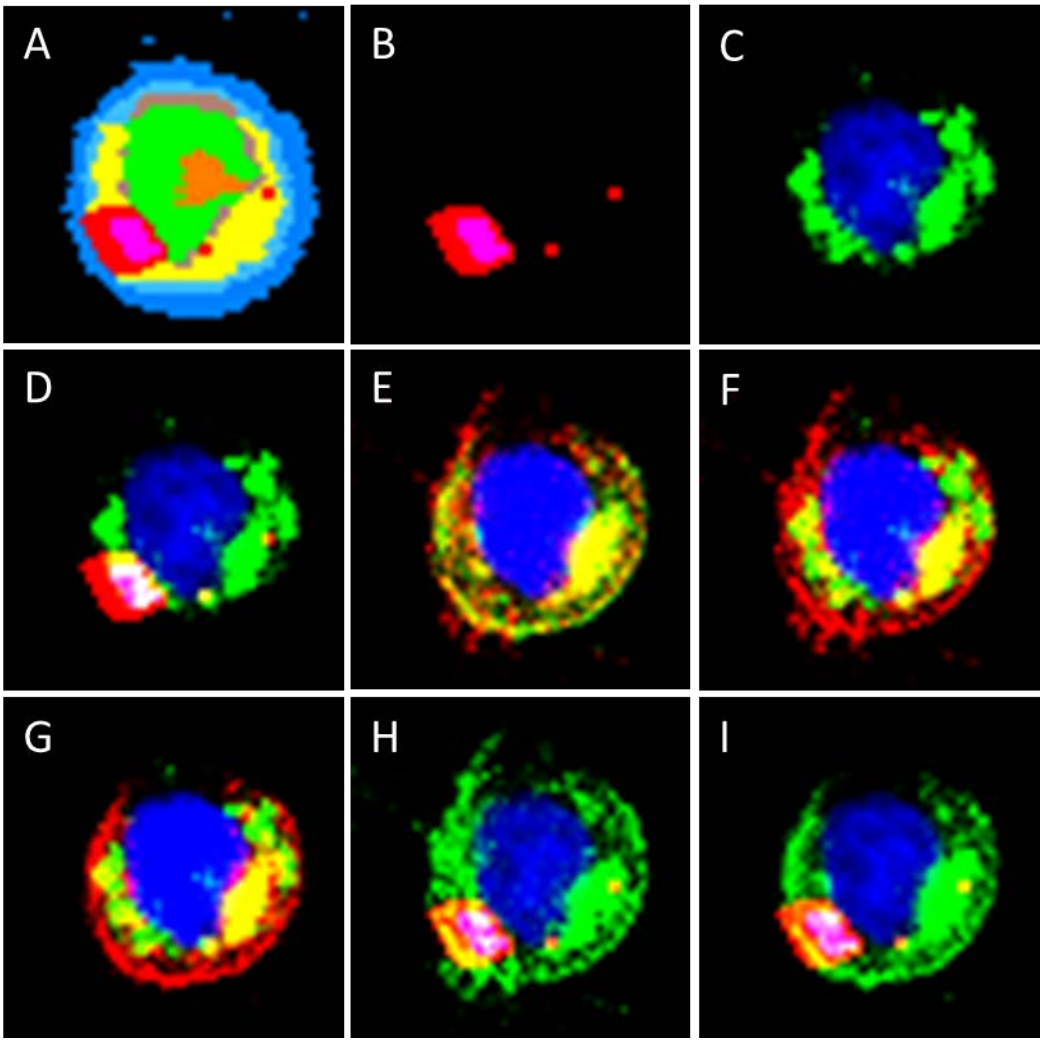

Figure S20. Raman and fluorescence imaging of SK-BR-3 cell treated with 5 μM neratinib for 8h. (A) HCA of the Raman results of the cell. (B) HCA of neratinib-containing clusters in the cell, (C) fluorescence image of the same cell that shows lysosomes (green) surrounding the nucleus (blue), and (D) an overlay (yellow and white) of (B) and (C). (E) Fluorescence image of the same cell that shows EGFR (red) and HER2 (green) distribution around the nucleus. An overlay (yellow) of (C) with EGFR (red) and HER2 (red) is shown in Panels (F) and (G), respectively. An overlay (yellow and white) of (B) with EGFR (green) and HER2 (green) is also shown in Panels (H) and (I), respectively.

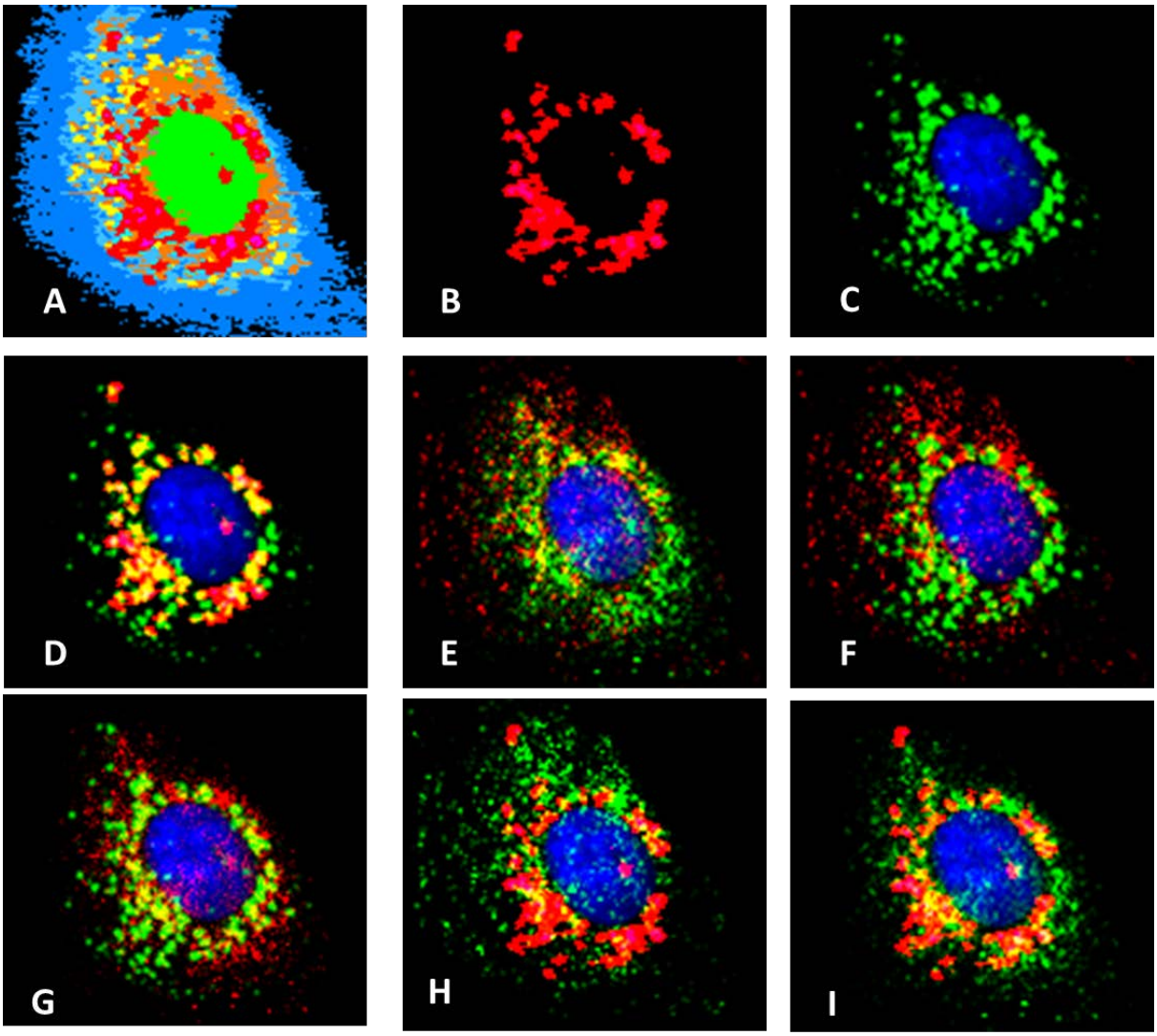

Figure S21. Raman and fluorescence imaging of NCI-H1975 cells treated with 5 μM neratinib for 8h. (A) HCA of the Raman results of the cell. (B) HCA of neratinib-containing clusters in the cell, (C) fluorescence image of the same cell that shows lysosomes (green) surrounding the nucleus (blue), and (D) an overlay (yellow and white) of (B) and (C). (E) Fluorescence image of the same cell that shows EGFR (red) and HER2 (green) distribution around the nucleus. An overlay (yellow) of (C) with EGFR (red) and HER2 (red) is shown in Panels (F) and (G), respectively. An overlay (yellow and white) of (B) with EGFR (green) and HER2 (green) is also shown in Panels (H) and (I), respectively.

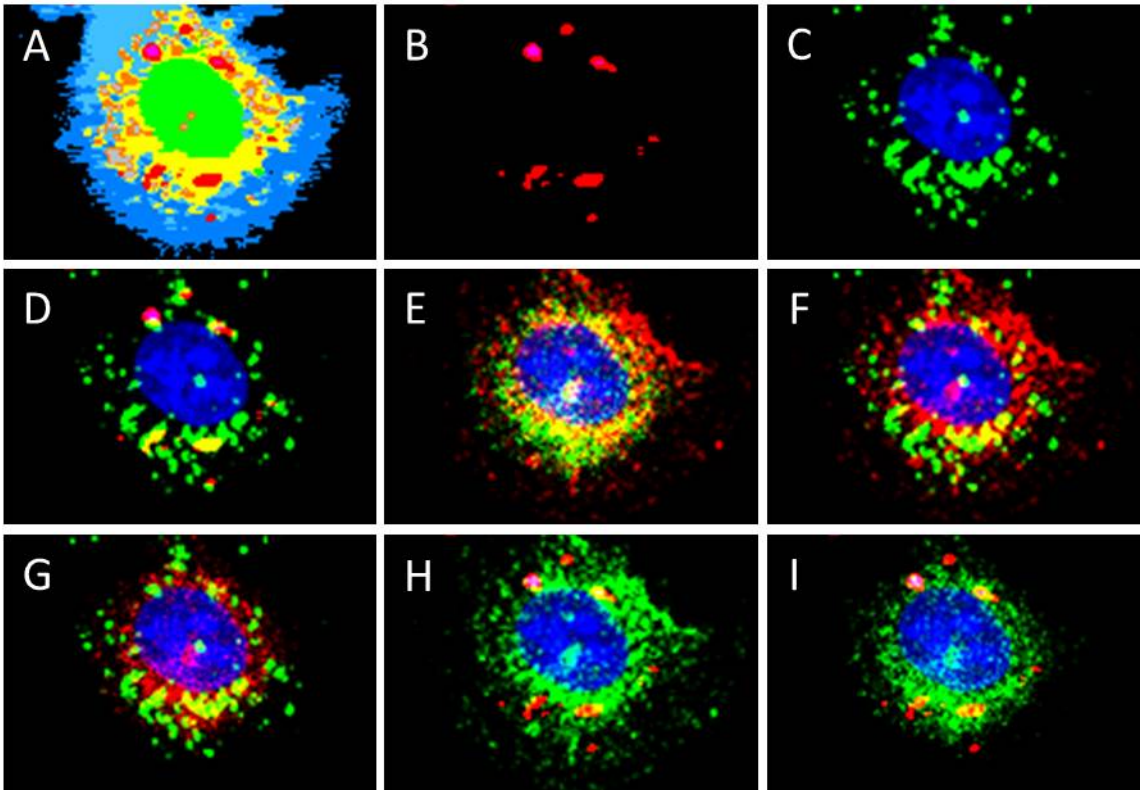

Figure S22. Raman and fluorescence imaging of NCI-H1975 cells treated with 5 μM neratinib for 8h. (A) HCA of the Raman results of the cell. (B) HCA of neratinib-containing clusters in the cell, (C) fluorescence image of the same cell that shows lysosomes (green) surrounding the nucleus (blue), and (D) an overlay (yellow and white) of (B) and (C). (E) Fluorescence image of the same cell that shows EGFR (red) and HER2 (green) distribution around the nucleus. An overlay (yellow) of (C) with EGFR (red) and HER2 (red) is shown in Panels (F) and (G), respectively. An overlay (yellow and white) of (B) with EGFR (green) and HER2 (green) is also shown in Panels (H) and (I), respectively.

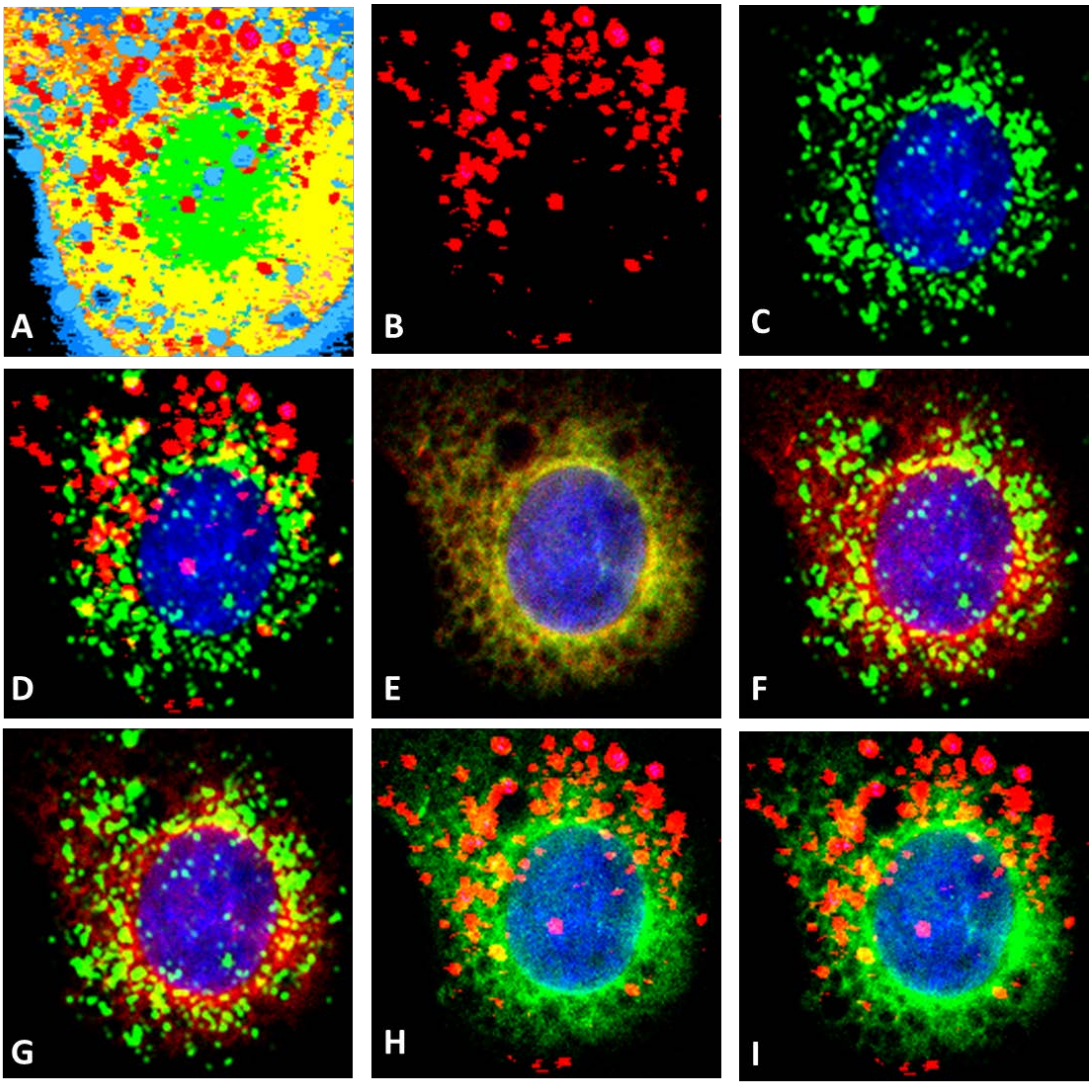

Figure S23. Raman and fluorescence imaging of NCI-H1975 cells treated with 5 μM neratinib for 8h. (A) HCA of the Raman results of the cell. (B) HCA of neratinib-containing clusters in the cell, (C) fluorescence image of the same cell that shows lysosomes (green) surrounding the nucleus (blue), and (D) an overlay (yellow and white) of (B) and (C). (E) Fluorescence image of the same cell that shows EGFR (red) and HER2 (green) distribution around the nucleus. An overlay (yellow) of (C) with EGFR (red) and HER2 (red) is shown in Panels (F) and (G), respectively. An overlay (yellow and white) of (B) with EGFR (green) and HER2 (green) is also shown in Panels (H) and (I), respectively.

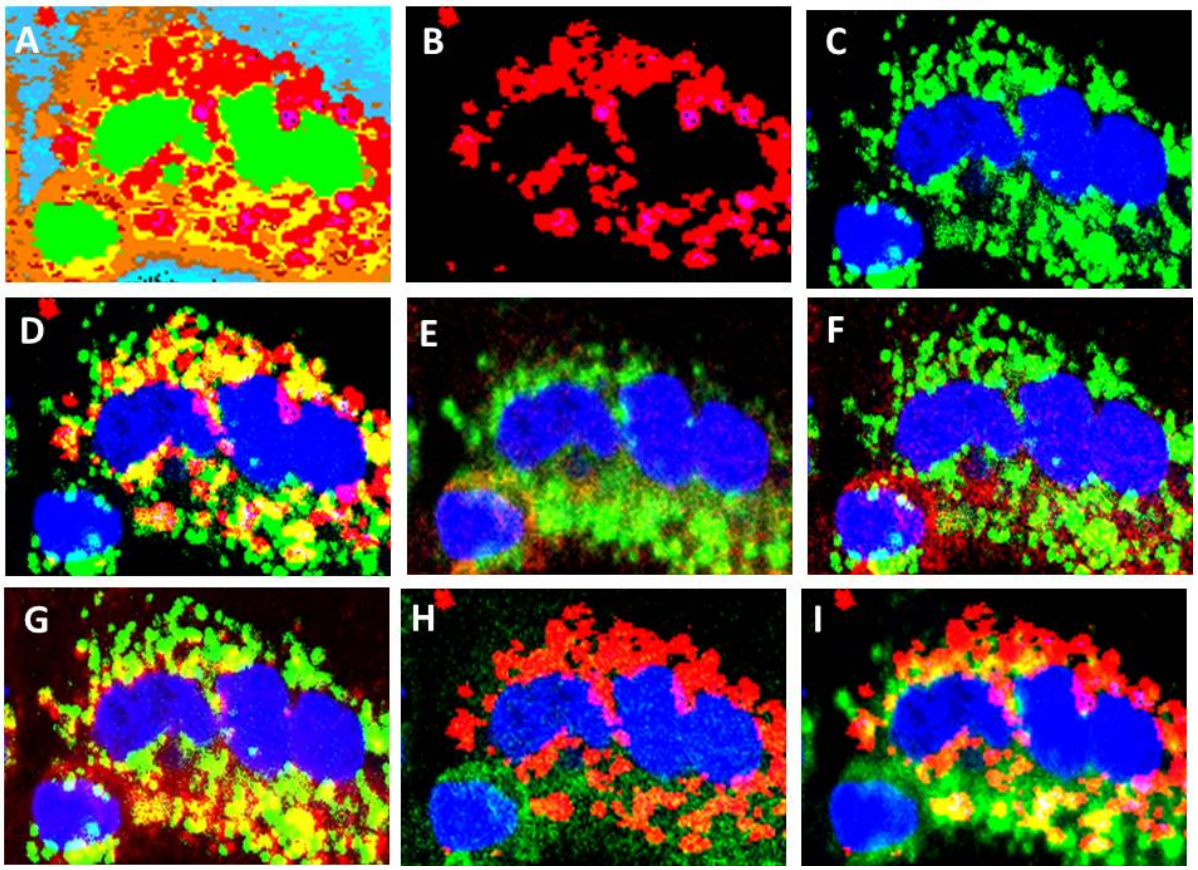

Figure S24. Raman and fluorescence imaging of Calu-3 cells treated with 5 μM neratinib for 8h. (A) HCA of the Raman results of cells. (B) HCA of neratinib-containing clusters in the cell, (C) fluorescence image of the same cells that shows lysosomes (green) surrounding the nucleus (blue), and (D) an overlay (yellow and white) of (B) and (C). (E) Fluorescence image of the same cells that shows EGFR (red) and HER2 (green) distribution around the nucleus. An overlay (yellow) of (C) with EGFR (red) and HER2 (red) is shown in Panels (F) and (G), respectively. An overlay (yellow and white) of (B) with EGFR (green) and HER2 (green) is also shown in Panels (H) and (I), respectively.

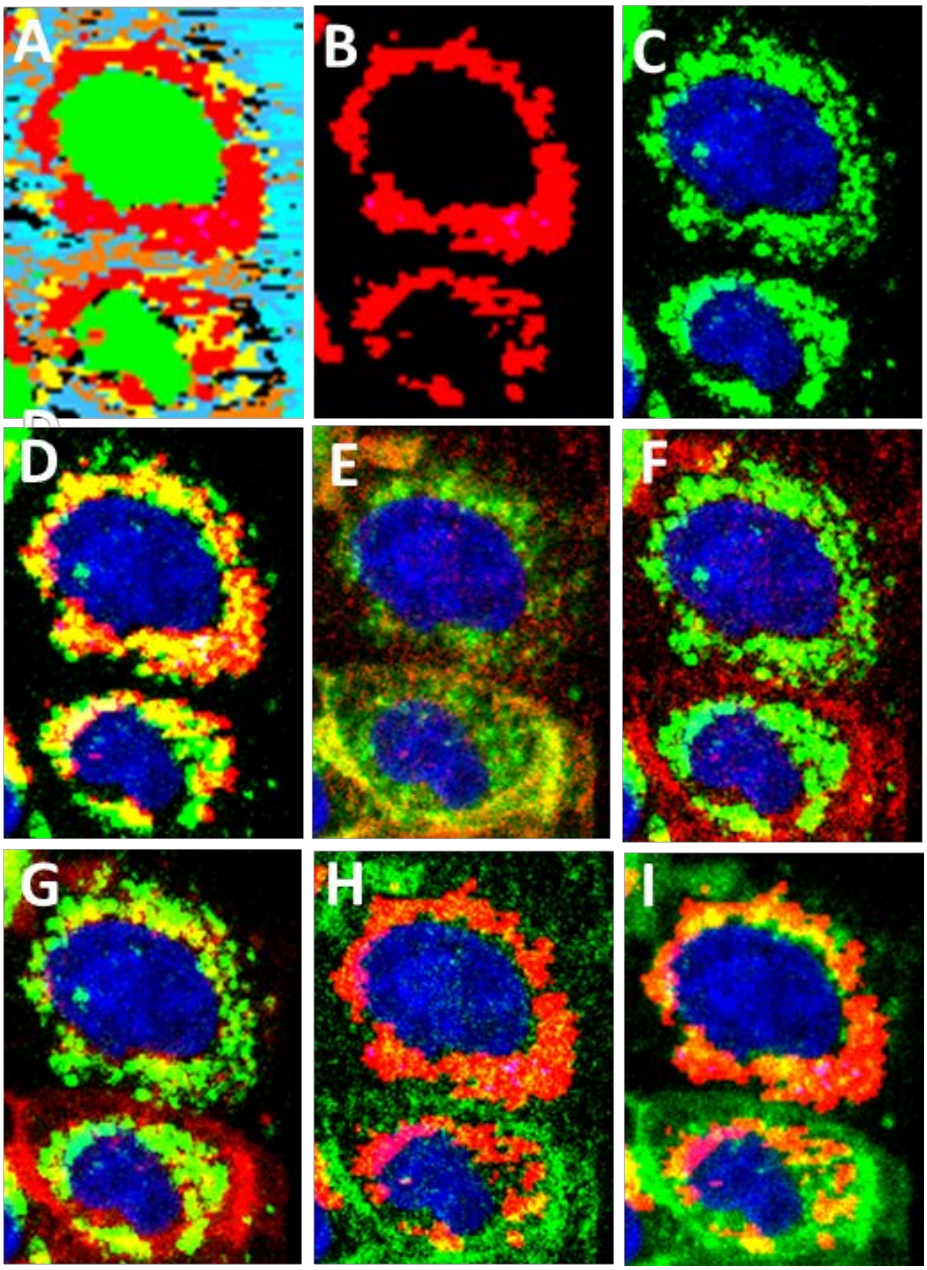

Figure S25. Raman and fluorescence imaging of Calu-3 cells treated with 5 μM neratinib for 8h. (A) HCA of the Raman results of cells. (B) HCA of neratinib-containing clusters in the cell, (C) fluorescence image of the same cells that shows lysosomes (green) surrounding the nucleus (blue), and (D) an overlay (yellow and white) of (B) and (C). (E) Fluorescence image of the same cells that shows EGFR (red) and HER2 (green) distribution around the nucleus. An overlay (yellow) of (C) with EGFR (red) and HER2 (red) is shown in Panels (F) and (G), respectively. An overlay (yellow and white) of (B) with EGFR (green) and HER2 (green) is also shown in Panels (H) and (I), respectively.

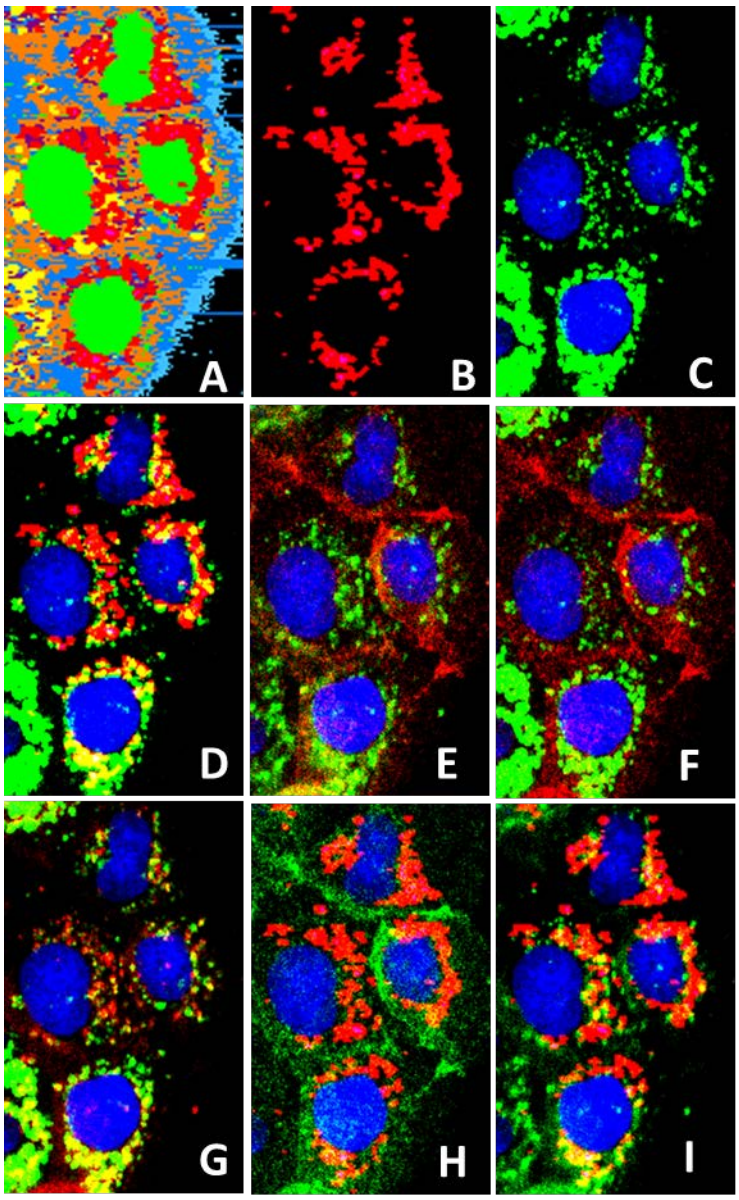

Figure S26. Raman and fluorescence imaging of Calu-3 cells treated with 5 μM neratinib for 8h. (A) HCA of the Raman results of cells. (B) HCA of neratinib-containing clusters in the cell, (C) fluorescence image of the same cells that shows lysosomes (green) surrounding the nucleus (blue), and (D) an overlay (yellow and white) of (B) and (C). (E) Fluorescence image of the same cells that shows EGFR (red) and HER2 (green) distribution around the nucleus. An overlay (yellow) of (C) with EGFR (red) and HER2 (red) is shown in Panels (F) and (G), respectively. An overlay (yellow and white) of (B) with EGFR (green) and HER2 (green) is also shown in Panels (H) and (I), respectively.

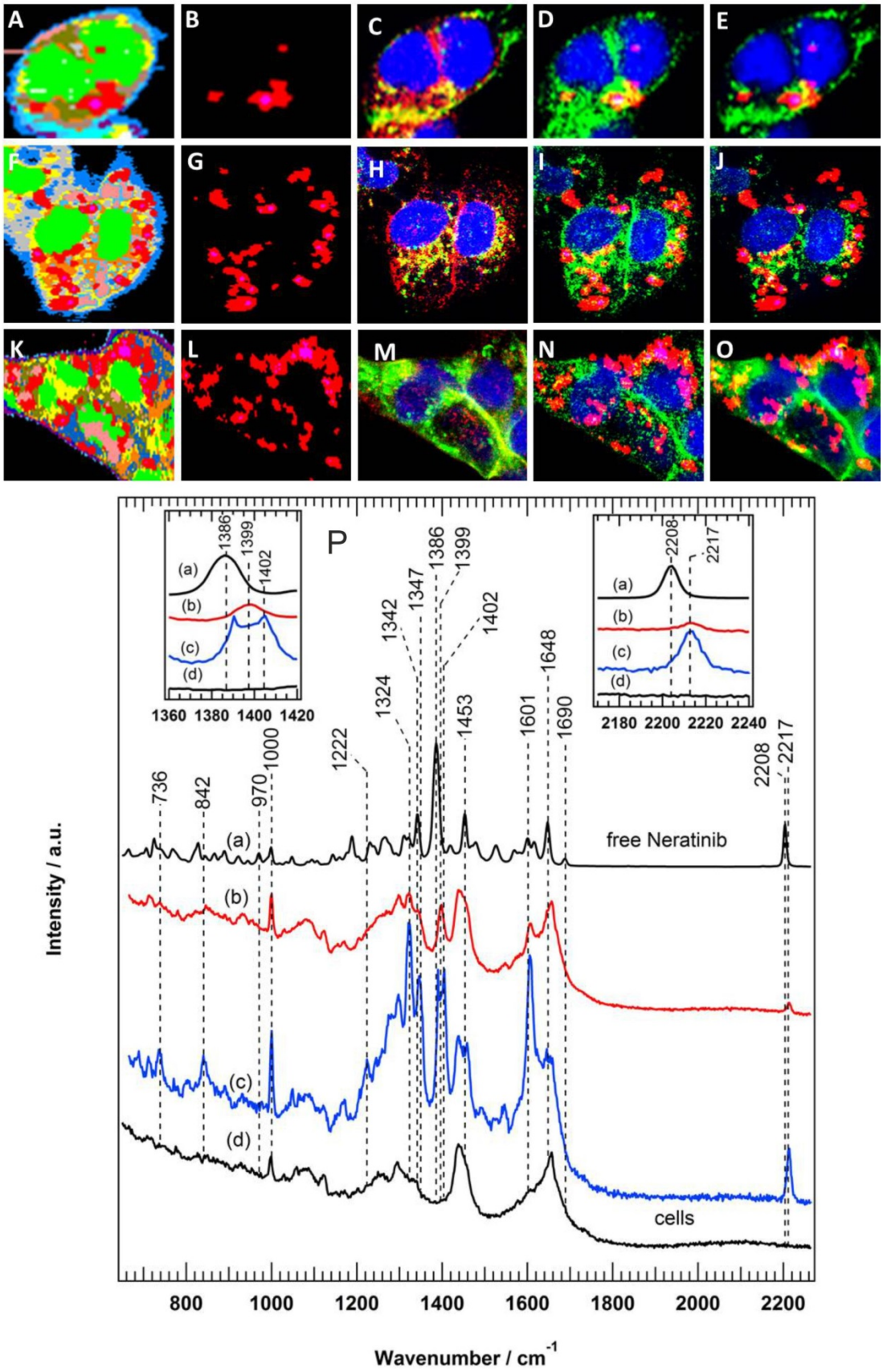

Figure S27. Raman measurements of cancer cells treated with 5 μM neratinib for 8h in the absence of LysoTracker staining. (A) HCA of the Raman results of SK-BR-3 cells. (B) HCA clusters of the only neratinib in cells. (C) Fluorescence image of the same cells that shows the

distribution of EGFR (red) and HER2 (green) around the nucleus (blue). (D) An overlay (yellow and white) of neratinib clusters (B) with fluorescence image of EGFR (green) and nucleus (blue). (E) An overlay (yellow and white) of neratinib clusters (B) with fluorescence image of HER2 (green) and nucleus (blue). Similar results were obtained for NCI-H1975 (F-J) and Calu-3 (K-O) cells. (P) Raman spectrum of free neratinib (a), the average Raman spectra of drug regions within the SK-BR-3 cells of the red (b) and blue (c) clusters in Panel (A) are shown in addition to the Raman spectrum of untreated SK-BR-3 cells (d). The insets of Panel (P) show enlarged spectra around 1386 and 2208 cm^{-1} bands.

These experiments were performed in the absence of LysoTracker in contrast to those presented in Figures 3 and S18-S26. The metabolites M1 and M2 in Panel (P) were detected in these measurements similar to those observed in the presence of LysoTracker (Figures 3 and S18-S26). This means that LysoTracker has no significant effect on the Raman results.

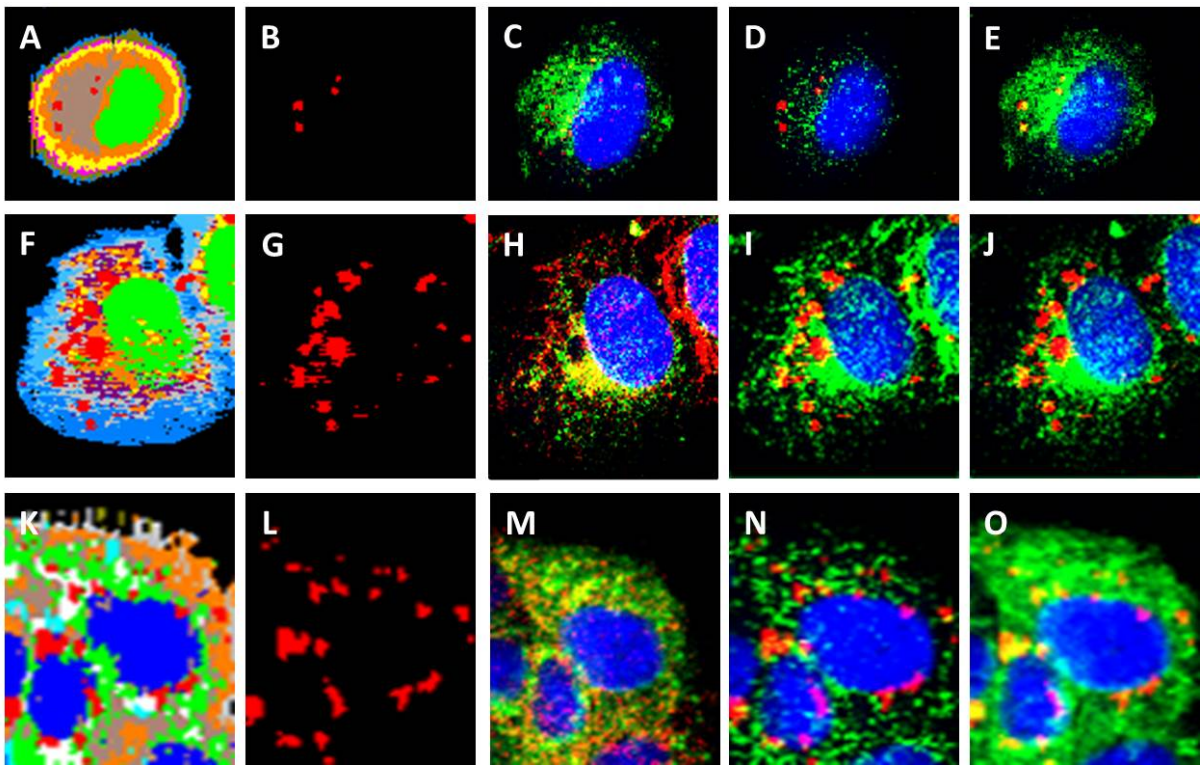

Figure S28. Raman measurements of cancer cells treated with 1 µM neratinib for 8h in the absence of LysoTracker staining. (A) HCA of the Raman results of the SK-BR-3 cell. (B) HCA clusters of the only neratinib in the cell. (C) Fluorescence image of the same cells that shows the distribution of EGFR (red) and HER2 (green) around the nucleus (blue). (D) An overlay (yellow) of the neratinib cluster (B) with fluorescence image of EGFR (green) and nucleus (blue). (E) An overlay (yellow) of the neratinib cluster (B) with fluorescence image of HER2 (green) and nucleus (blue). Similar results were obtained for NCI-H1975 (F-J) and Calu-3 (K-O) cells.

These experiments were performed in the absence of LysoTracker. Only one metabolite (M1) was detected by using 1 µM neratinib in these measurements, while 5µM neratinib concentration was used in Figures 3 and S18-S26.

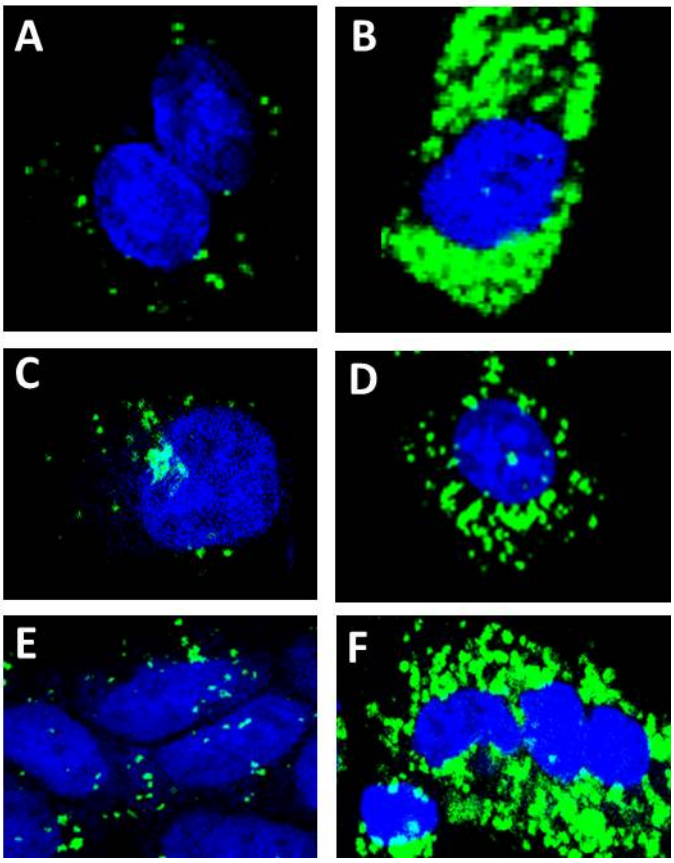

Figure S29. Fluorescence imaging of lysosomes (green) and nucleus (blue) of SK-BR-3 cells (A-B), NCI-H1975 (C-D), and Calu-3 (E-F) cells. Cells in Panels, (A,C,E) were not treated with neratinib (control), while those in Panels (B,D,F) were treated with 5 μM neratinib for 8h.

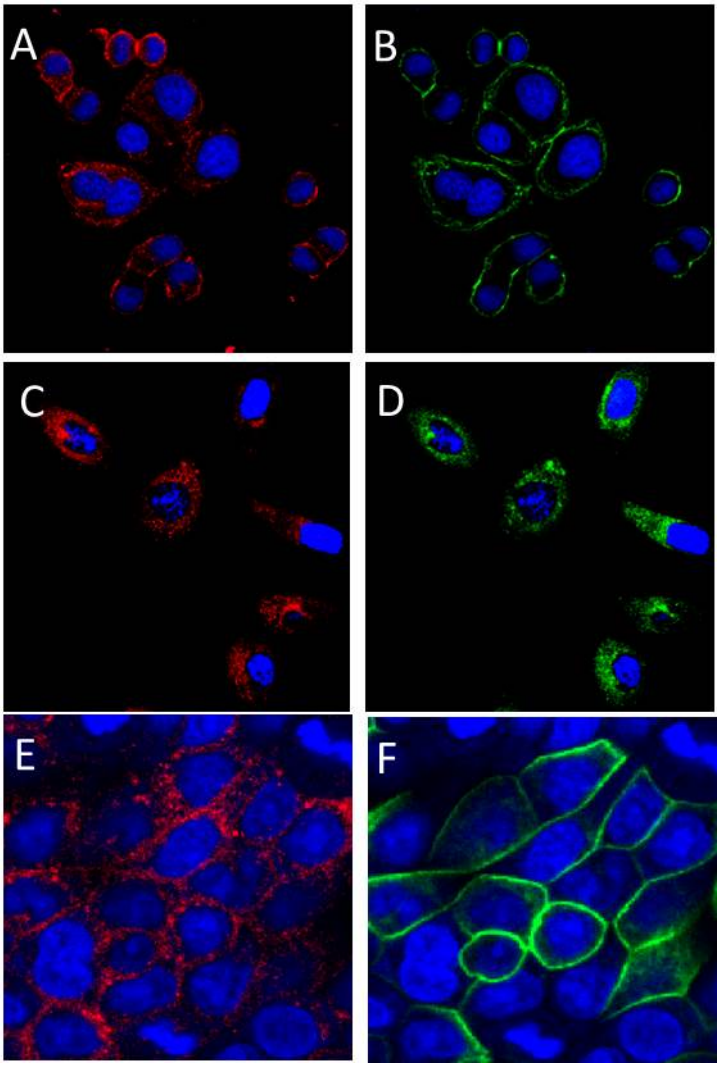

Figure S30. Fluorescence imaging of EGFR (red), HER2 (green) and nucleus (blue) of SK-BR-3 (A-B), NCI-H1975 (C-D), and Calu-3 (E-F) cells. These cells were not treated with neratinib.

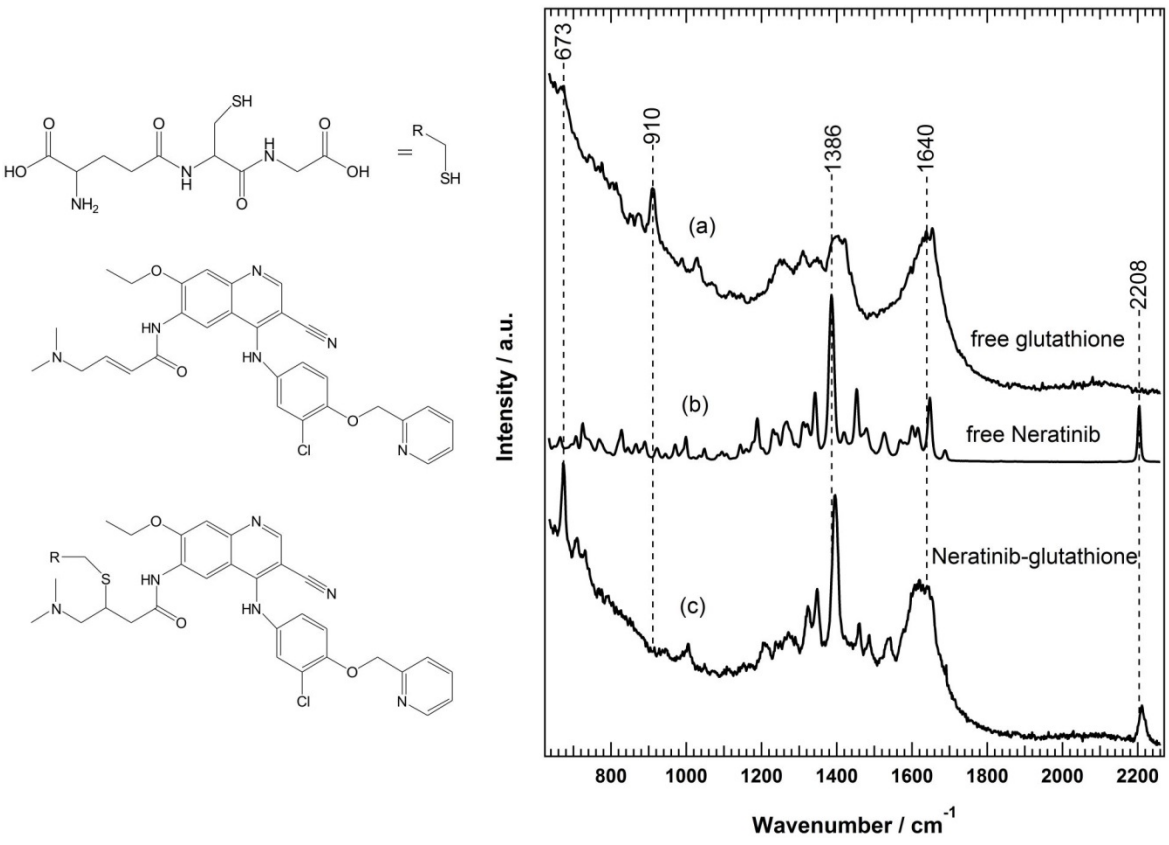

Figure S31. Raman spectra of free glutathione (a), free neratinib (b), and neratinib-glutathione adduct (c). The chemical structures of glutathione, neratinib and neratinib-glutathione adduct are also displayed.

It is noted that we could not monitor the reactivity of neratinib with the recombinant EGFR protein by Raman microscopy because the Raman signal of EGFR (0.34 mg/50 µL) was not detectable.

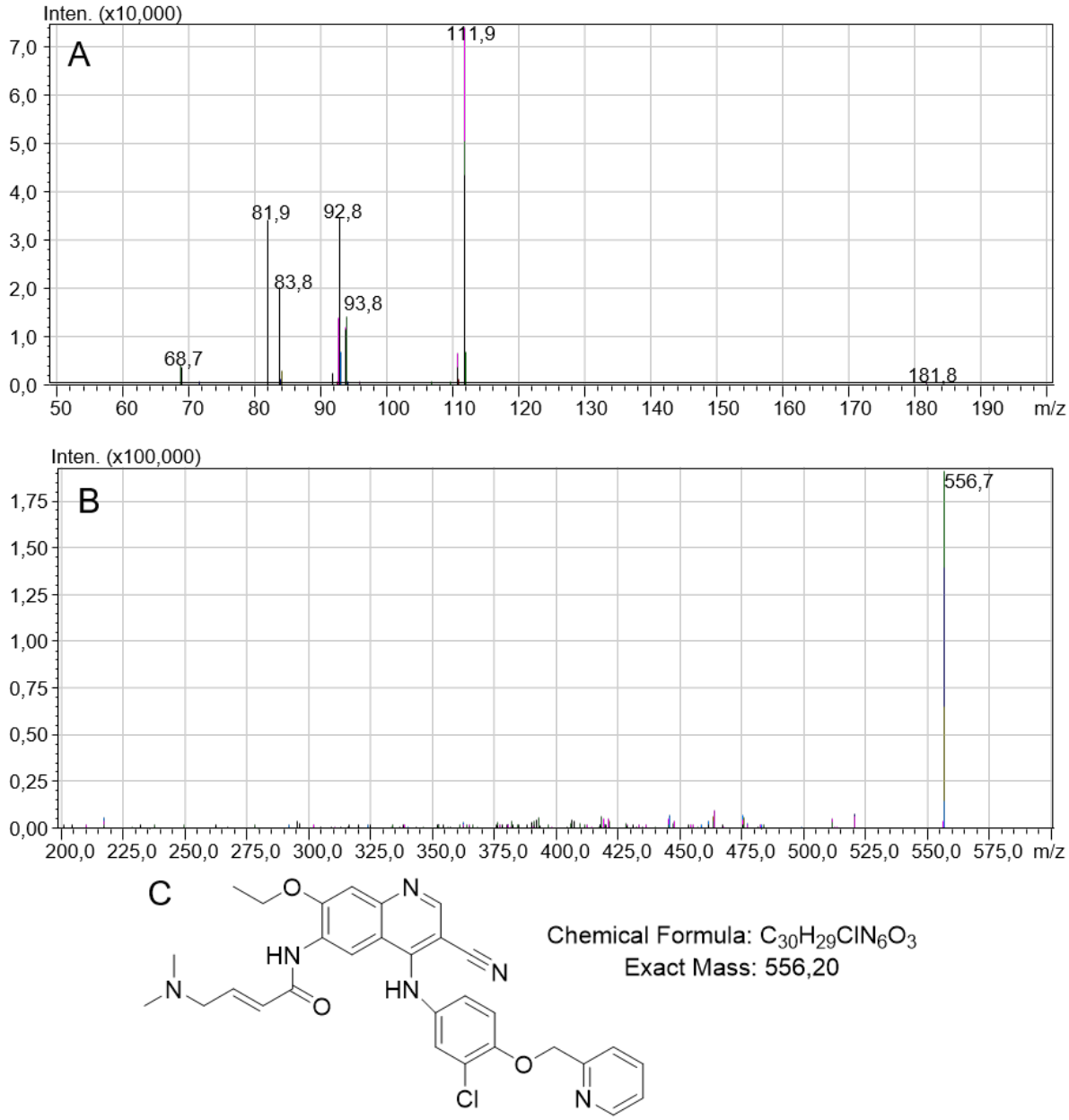

Figure S32. MS/MS data of product ion scan (PIS) experiments on neratinib without cellular matrix. Experiments were carried out from the precursor ion *m/z* = 557.4 $[M+H]^+$ at collision energies ranging from 2-40 V. Fragmentation data was detected in the *m/z* ranges of (A) 50-205 and (B) 200-600. Overlays of all fragmentation data are given in absolute intensity mode. The structure and exact mass of neratinib are given as reference (C).

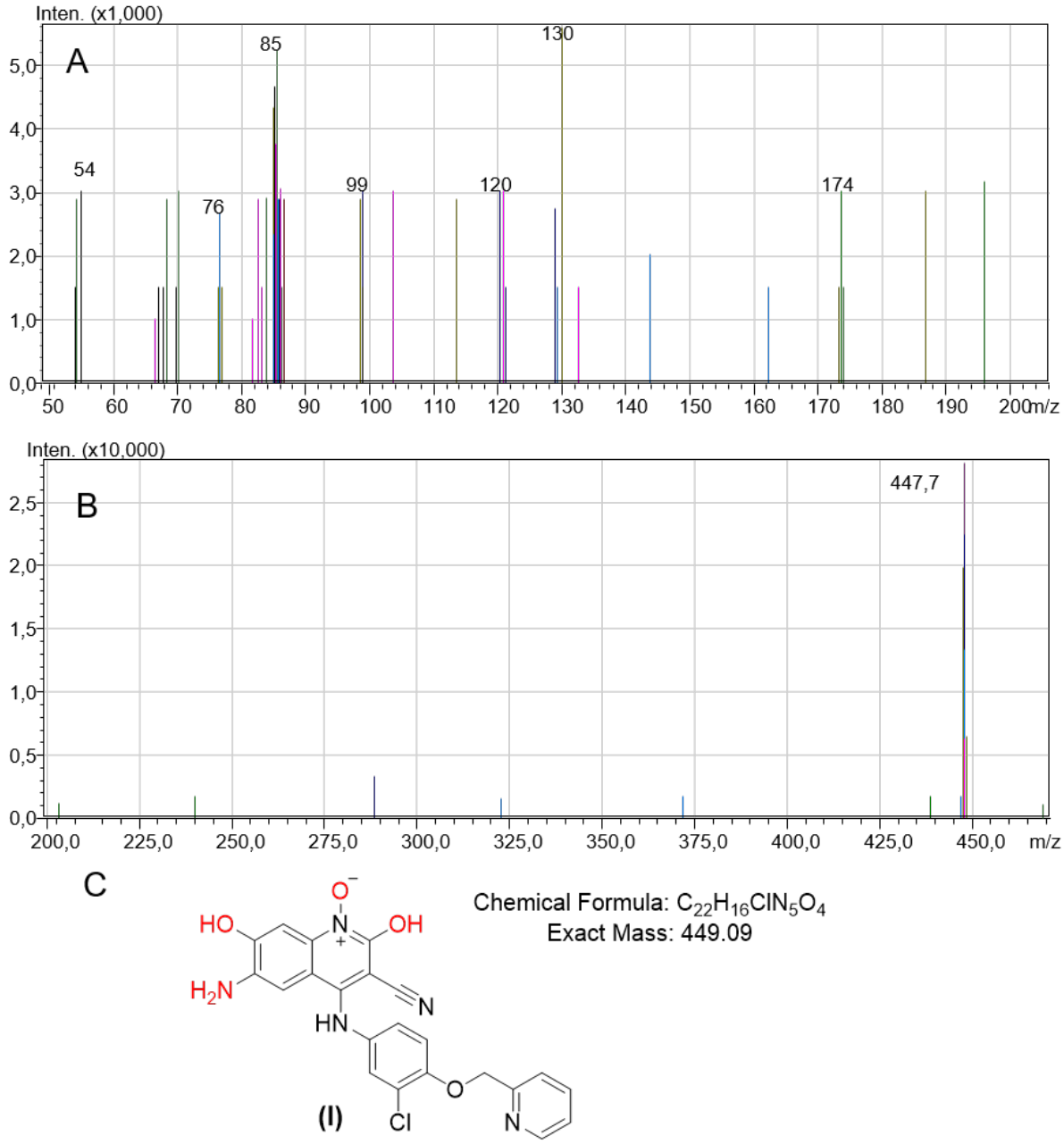

Figure S33. MS/MS data of representative product ion scan (PIS) experiments on metabolite (I) within the cytosol fraction of SK-BR-3 cells. Experiments were carried out from the precursor ion *m/z* = 450.1 $[M+H]^+$ at collision energies ranging from 2-40 V. Fragmentation data was detected in the *m/z* ranges of (A) 50-205 and (B) 200-600. Overlays of all fragmentation data are given in absolute intensity mode. The structure and exact mass of metabolite **I** are given as reference (C).

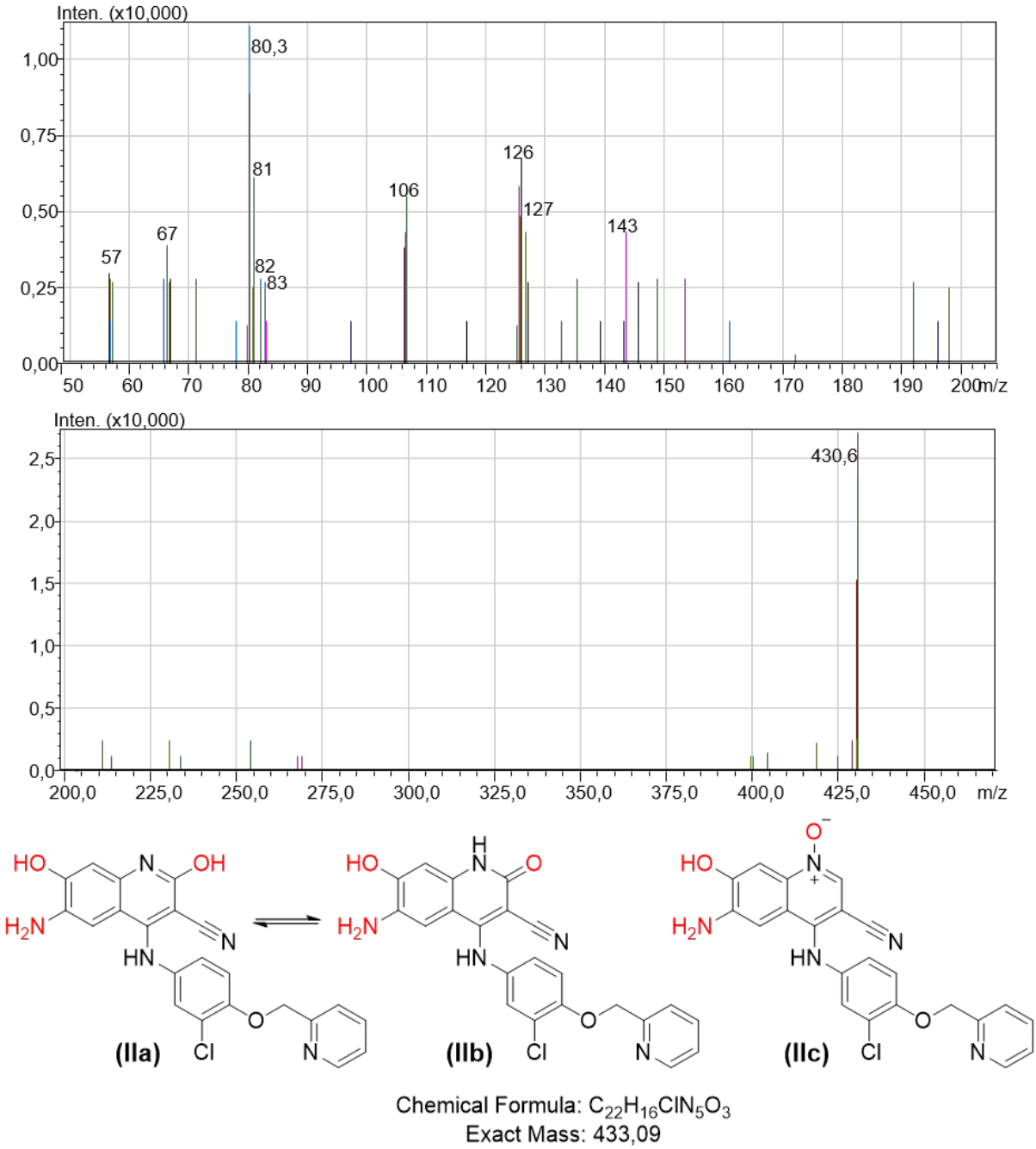

Figure S34. MS/MS data of representative product ion scan (PIS) experiments on metabolite (I) within the cytosol fraction of SK-BR-3 cells. Experiments were carried out from the precursor ion *m/z* = 433.1 $[M]^+$ at collision energies ranging from 2-40 V. Fragmentation data was detected in the *m/z* ranges of (A) 50-205 and (B) 200-600. Overlays of all fragmentation data are given in absolute intensity mode. The structure and exact mass of metabolite isomers **IIa-IIc** are given as reference (C).

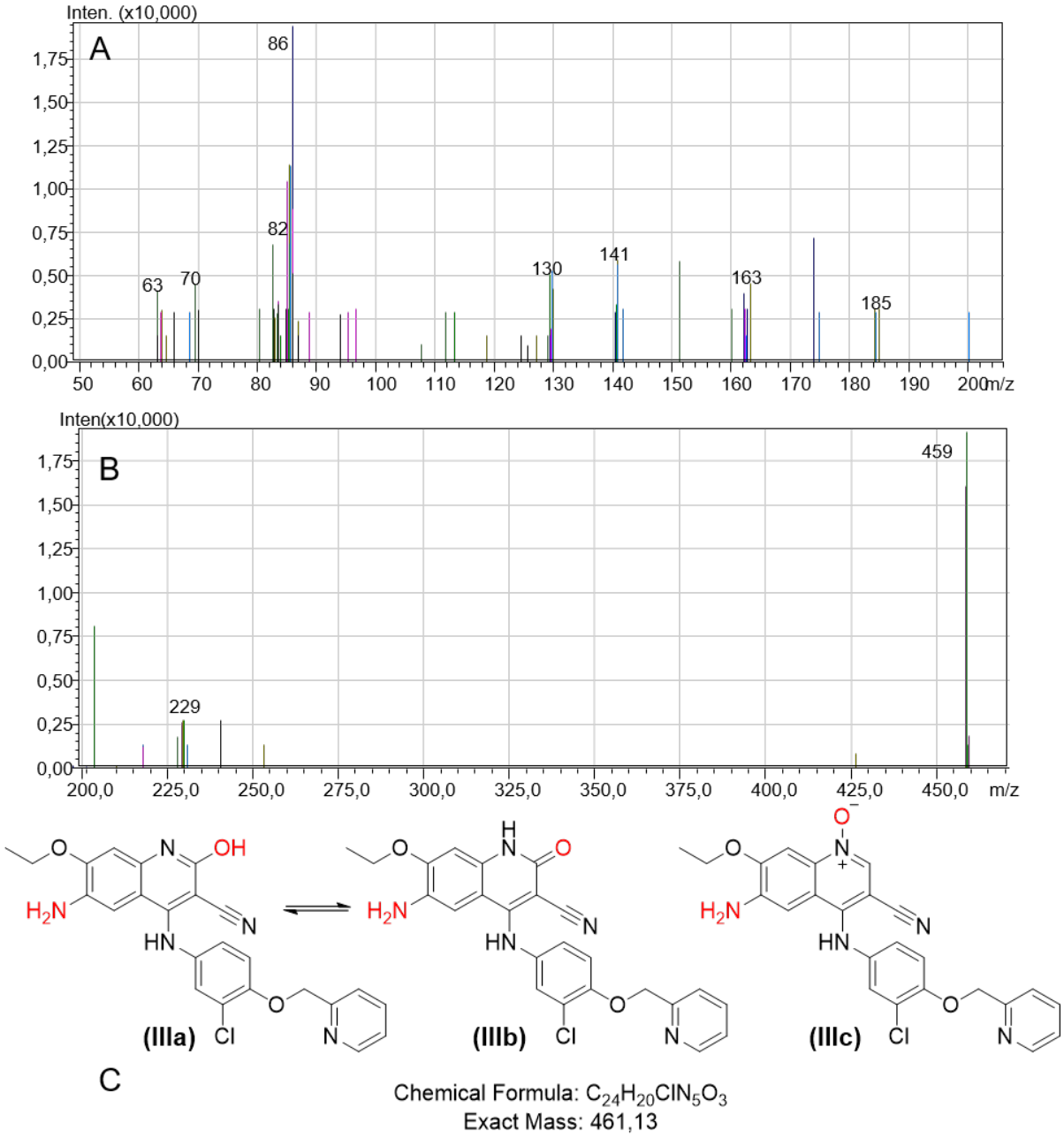

Figure S35. MS/MS data of representative product ion scan (PIS) experiments on metabolite (I) within the cytosol fraction of SK-BR-3 cells. Experiments were carried out from the precursor ion *m/z* = 461.1 $[M]^+$ at collision energies ranging from 2-40 V. Fragmentation data was detected in the *m/z* ranges of (A) 50-205 and (B) 200-600. Overlays of all fragmentation data are given in absolute intensity mode. The structure and exact mass of metabolite isomers **IIIa-IIIc** are given as reference (C).

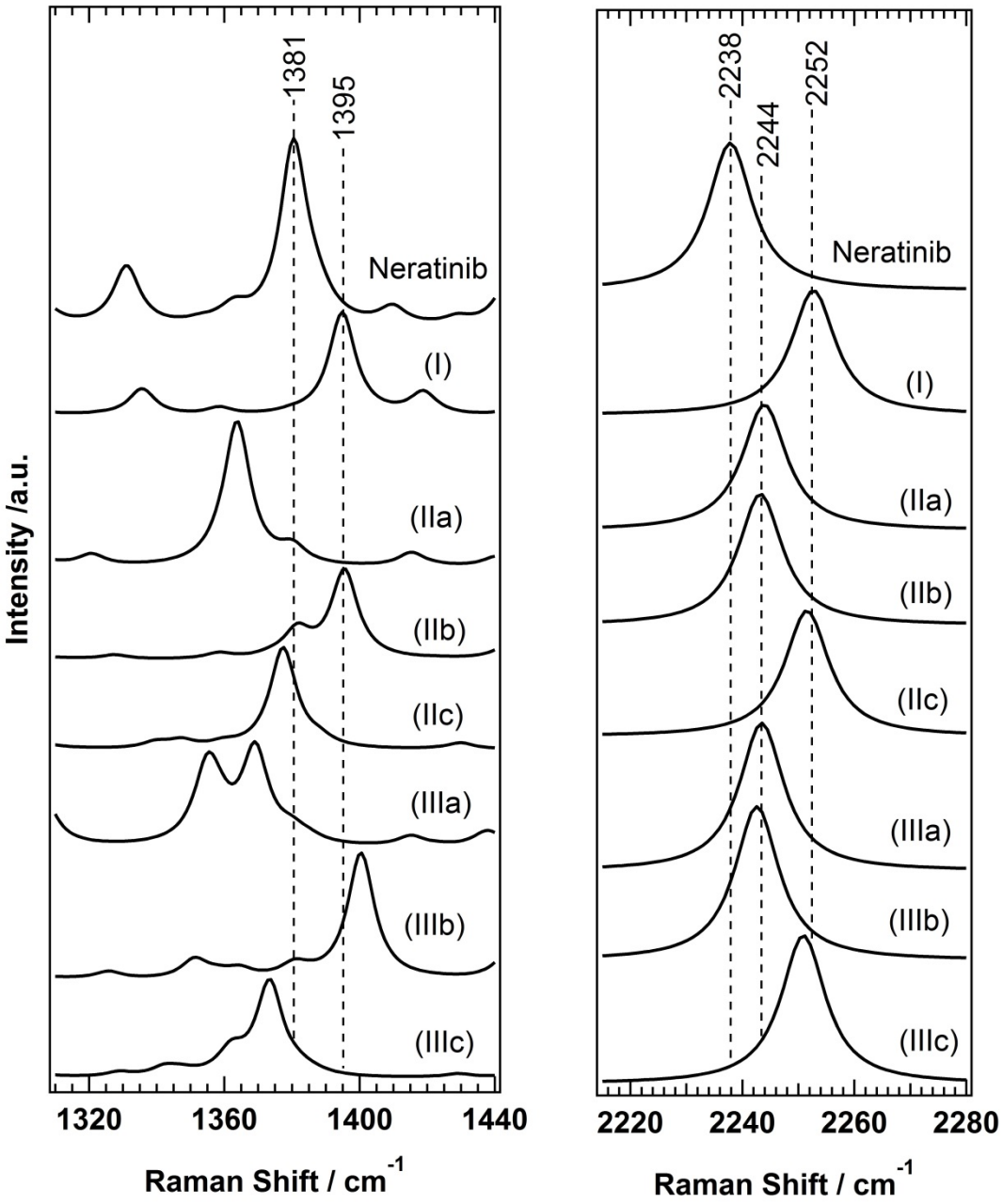

Figure S36. DFT calculations of the Raman spectra of metabolite candidates of neratinib in the marker regions. The structures of these candidates are shown in Scheme 1.

The Raman results indicate that the 1386 and 2208 cm^{-1} bands of free neratinib are upshifted by +13 and +9 cm^{-1}, respectively, in the M1 Raman spectrum. The DFT calculations revealed similar wavenumber shifts only for Metabolite I, while other candidates show either

wavenumber downshift and/or an appearance of a new Raman band near 1400 cm^{-1}. Therefore, we suggest that M1 Raman spectrum originates from metabolite I.

Furthermore, the band at 2208 cm^{-1} is upshifted to 2217 cm^{-1} (+9) in the M2 Raman spectrum metabolite (Figures 2, S2-S3). In addition, a doublet at 1388 (+2)/1402 (+16) cm^{-1} appeared instead of a single band at 1386 cm^{-1} in the spectrum of free neratinib. Similar wavenumber shifts and presence of doublet bands near 1382/1395 were detected in both metabolites IIb and IIIb by DFT calculations. Since the chemical structure of these metabolite candidates is similar, we suggest that metabolites IIb and/or IIIb contribute to the Raman spectrum of M2.

“We also have calculated the Raman spectra of some aromatic molecules, neratinib fragments as well as the Raman spectrum of erlotinib,[1] and compared the data with the calculated Raman spectrum of neratinib. It is clear that the intensity of the Raman bands of neratinib is much higher than those of the aromatic molecules (Figure S37) and erlotinib (Figure S38), especially in the fingerprint region. Furthermore, increasing the π-system in the substituents of the quinoline ring at positions 4 and 6 is responsible for the enhancement of the Raman intensity of neratinib, as can be seen in Figure S39. This is because removing these substituents leads to significantly reduce the intensity of the Raman bands of neratinib fragments. Therefore, we suggest that the strong Raman signals of neratinib in cells treated with low drug concentration are attributed mainly to the intracellular accumulation of neratinib at higher concentration and partially to the chemical structure of neratinib in comparison with other aromatic molecules.”

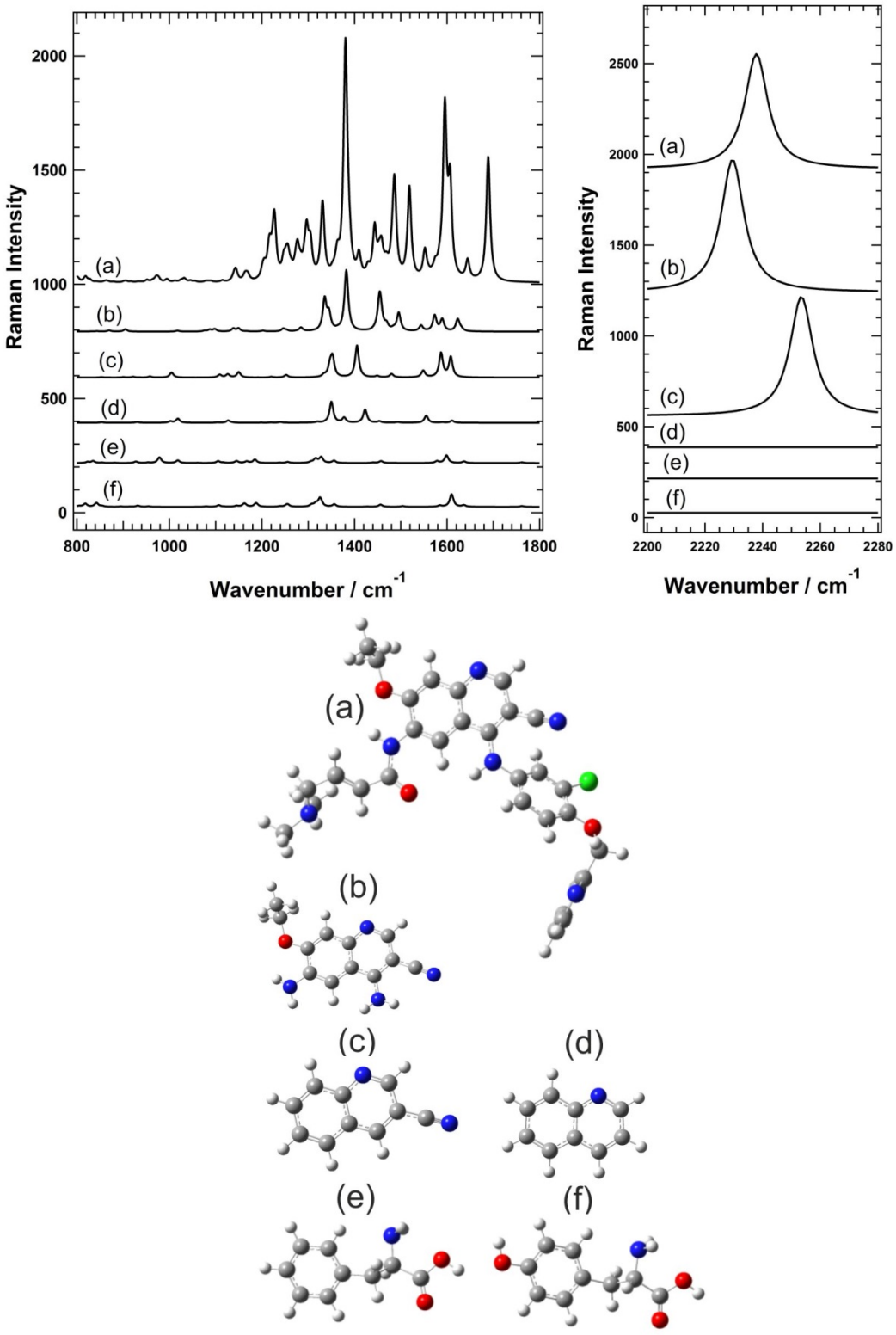

Figure S37. DFT calculations of the Raman spectra of (a) neratinib, (b) 3-cyano-4,6 diamino-7-ethoxy quinoline, (c) 3-cyanoquinoline, (d) quinoline, (e) Phe, and (f) Tyr. The chemical structures of these compounds are also displayed.

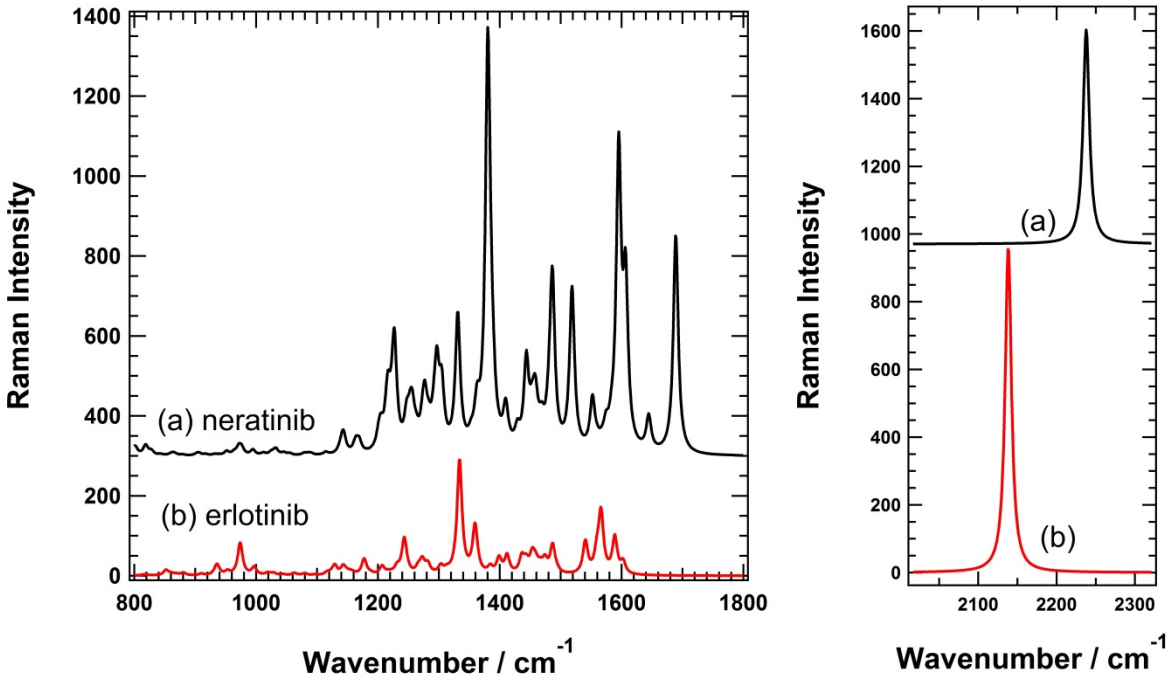

Figure S38. DFT calculations of the Raman spectra of (a) neratinib and (b) erlotinib.

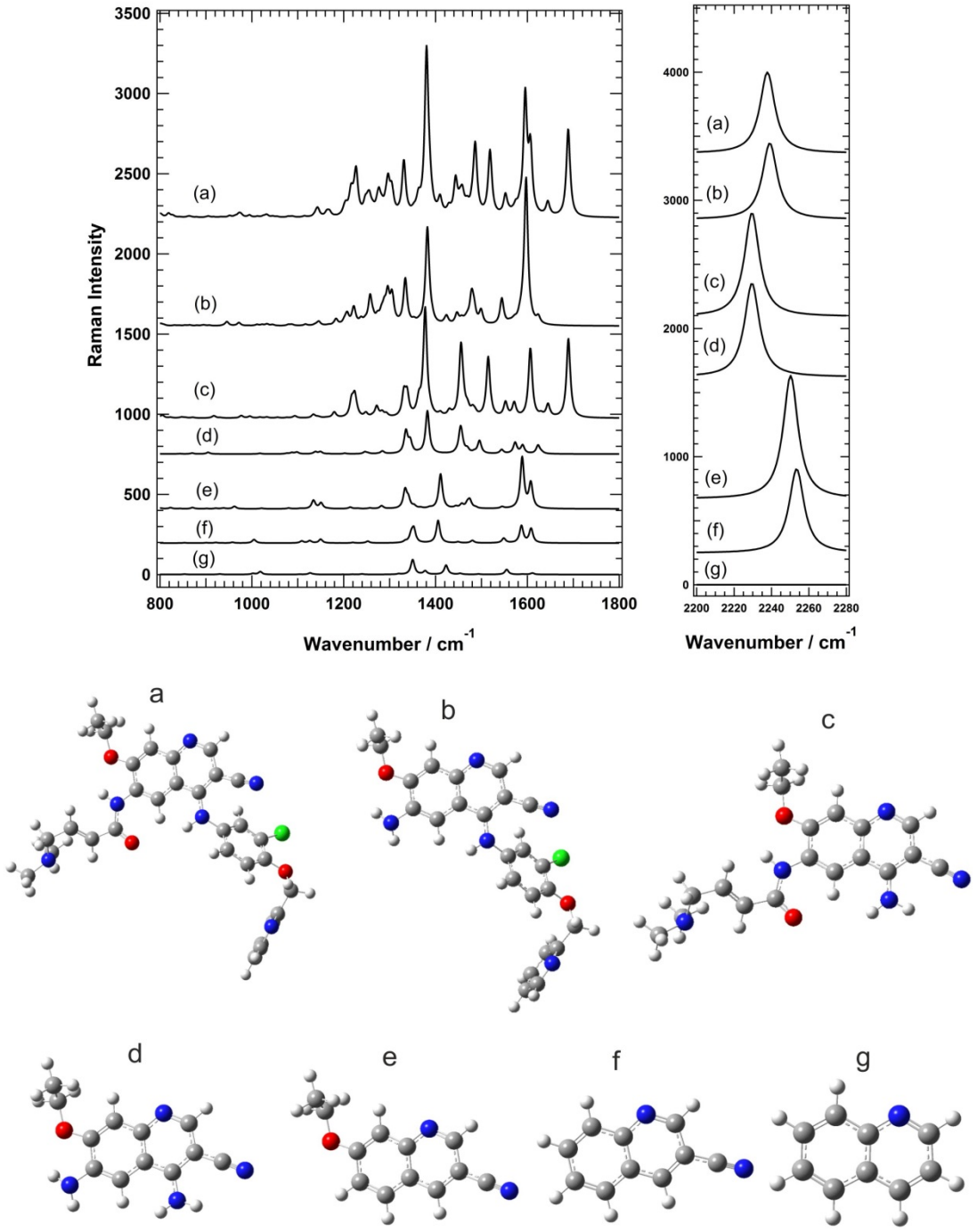

Figure S39. DFT calculations of the Raman spectra of neratinib fragments. The chemical structures of these fragments are also displayed.

References

[1] S. F. El-Mashtoly, D. Petersen, H. K. Yosef, A. Mosig, A. Reinacher-Schick, C. Kötting, K. Gerwert, *The Analyst* **2014**, *139*, 1155–1161.

[2] S. F. El-Mashtoly, H. K. Yosef, D. Petersen, L. Mavarani, A. Maghnouj, S. Hahn, C. Kötting, K. Gerwert, *Anal. Chem.* **2015**, *87*, 7297–7304.

[3] Y. Shibata, M. Chiba, *Drug Metab. Dispos. Biol. Fate Chem.* **2015**, *43*, 375–384.

[4] D. Fu, J. Zhou, W. S. Zhu, P. W. Manley, Y. K. Wang, T. Hood, A. Wylie, X. S. Xie, *Nat. Chem.* **2014**, *6*, 614–622.